



# LUND UNIVERSITY

## Kinetic and Thermodynamic Modeling of Nanowire Growth

Mårtensson, Erik

2021

*Document Version:*  
Other version

[Link to publication](#)

*Citation for published version (APA):*

Mårtensson, E. (2021). *Kinetic and Thermodynamic Modeling of Nanowire Growth*. Department of Physics, Lund University.

*Total number of authors:*

1

### General rights

Unless other specific re-use rights are stated the following general rights apply:

Copyright and moral rights for the publications made accessible in the public portal are retained by the authors and/or other copyright owners and it is a condition of accessing publications that users recognise and abide by the legal requirements associated with these rights.

- Users may download and print one copy of any publication from the public portal for the purpose of private study or research.
- You may not further distribute the material or use it for any profit-making activity or commercial gain
- You may freely distribute the URL identifying the publication in the public portal

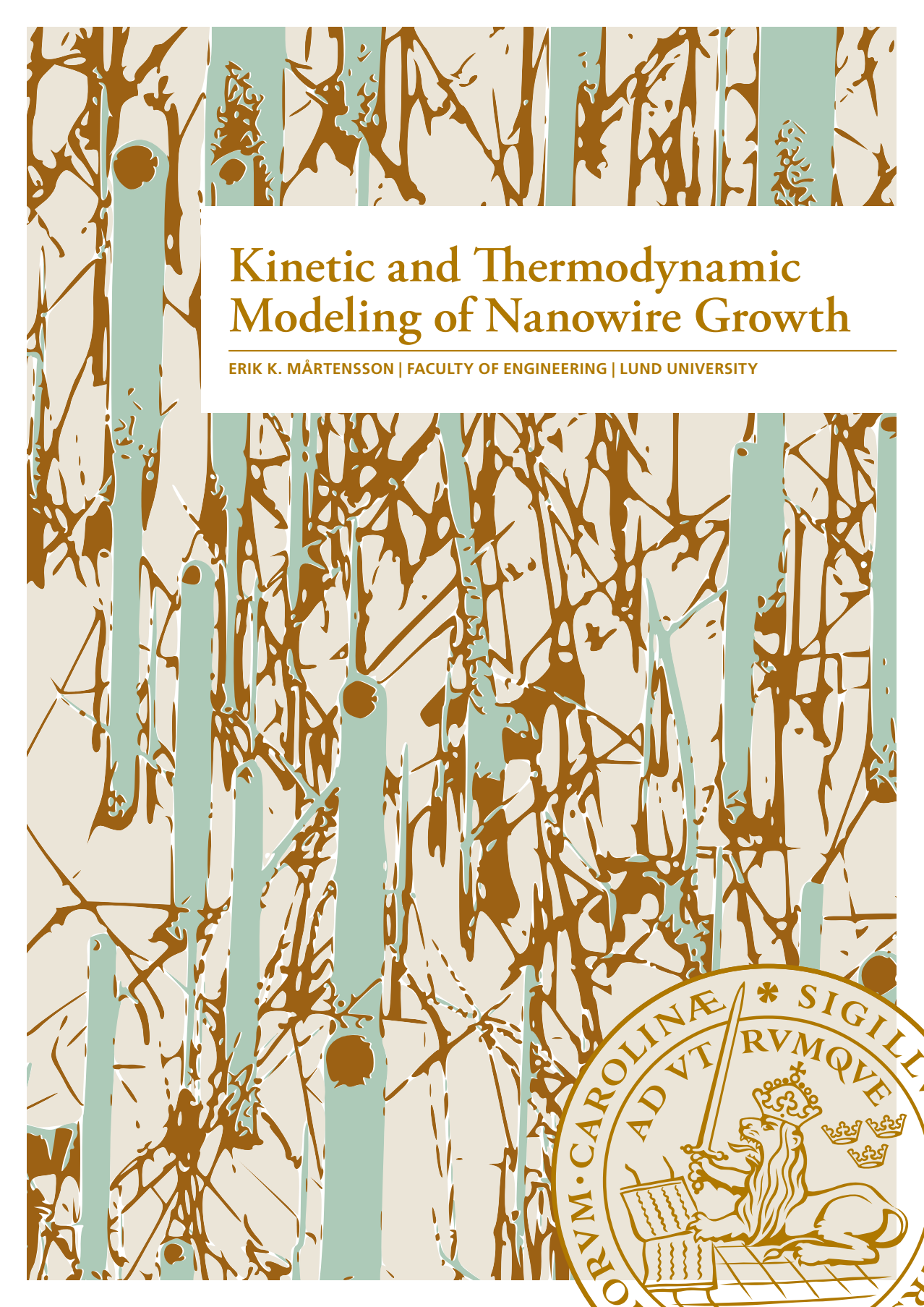
Read more about Creative commons licenses: <https://creativecommons.org/licenses/>

### Take down policy

If you believe that this document breaches copyright please contact us providing details, and we will remove access to the work immediately and investigate your claim.

LUND UNIVERSITY

PO Box 117  
221 00 Lund  
+46 46-222 00 00



# Kinetic and Thermodynamic Modeling of Nanowire Growth

ERIK K. MÅRTENSSON | FACULTY OF ENGINEERING | LUND UNIVERSITY





Lund University  
Faculty of Engineering  
Department of Physics  
ISBN 978-91-8039-008-8



# Kinetic and Thermodynamic Modeling of Nanowire Growth

by Erik K. Mårtensson



**LUND**  
UNIVERSITY

## DOCTORAL DISSERTATION

which, by due permission of the Faculty of Engineering of Lund University, Sweden,  
will be publicly defended on Tuesday, the 26th of October 2021, at 13.15 in Rydbergssalen  
at the Department of Physics, Sölvegatan 14, Lund, Sweden

Faculty opponent:  
Prof. Peter W. Voorhees  
Northwestern University

Thesis advisors:  
Prof. Kimberly A. Dick, Prof. Jonas Johansson, Dr. Sebastian Lehmann

Organization <b>LUND UNIVERSITY</b> Department of Physics Box 118 SE-221 00 LUND Sweden		Document name <b>DOCTORAL DISSERTATION</b>	
		Date of disputation <b>2021-10-26</b>	
		Sponsoring organization	
Author(s) <b>Erik K. Mårtensson</b>			
Title and subtitle <b>Kinetic and Thermodynamic Modeling of Nanowire Growth</b>			
Abstract <p>This thesis aims to expand on the fundamental knowledge of crystal growth, selectively focusing on the area of particle-seeded nanowire growth in the III-V materials system. The growth process is complex. It typically occurs via the vapor-liquid-solid method, wherein growth material is supplied in the vapor phase, but the solidification process occurs dynamically, layer by layer, via an intermediary liquid particle. This intermediary phase makes it difficult to assess the correlation between these three phases, and how changes in the vapor phase affect the liquid phase and, in turn, the solidification of the nanowire.</p> <p>This thesis examines the correlation between the vapor, liquid and solid phases, and how the dynamics of the layer-by-layer growth affects the process. This is done in part by combining experimental nanowire growth using metal-organic vapor phase epitaxy with thermodynamic modeling. The main contributions have been in combining thermodynamics, mass transfer and crystal growth kinetics into kinetic Monte Carlo models, and using these models to gain insights into the growth process.</p> <p>The findings of this thesis can be used both to further develop future theoretical models, and to aid in the development of experimental growth, by providing fundamental insights of the growth process and the affects of varying the experimentally accessible process parameters.</p>			
Key words <b>Crystal Growth, Nanowires, Simulation, Monte Carlo, III-V, Polytypism</b>			
Classification system and/or index terms (if any)			
Supplementary bibliographical information		Language <b>English</b>	
ISSN and key title		ISBN 978-91-8039-008-8 (print) 978-91-8039-009-5 (pdf)	
Recipient's notes		Number of pages <b>175</b>	Price
		Security classification	

I, the undersigned, being the copyright owner of the abstract of the above-mentioned dissertation, hereby grant to all reference sources the permission to publish and disseminate the abstract of the above-mentioned dissertation.

Signature 

Date 2021-09-15

# Kinetic and Thermodynamic Modeling of Nanowire Growth

by Erik K. Mårtensson



**LUND**  
UNIVERSITY

Paper I Reproduced with permission from:  
Crystal Growth & Design 18 (11), 6702-6712 © American Chemical Society 2018  
Paper II Reproduced with permission from:  
Nano letters 19 (2), 1197-1203 © American Chemical Society 2019  
Paper III Reproduced with permission from:  
Crystal Growth & Design 20 (8), 5373-5379 © American Chemical Society 2020  
Paper IV Reproduced with permission from:  
ACS nano 14 (4), 3868-3875 © American Chemical Society 2020  
Paper V © The Authors 2021

**Cover illustration front:** Au-seeded GaAs nanowires, grown using metal-organic vapor phase epitaxy on a substrate patterned by electron beam lithography. False colored for effect.

Pages 1-70 © Erik K. Mårtensson 2021

Solid State Physics, Department of Physics

ISBN: 978-91-8039-008-8 (print)

ISBN: 978-91-8039-009-5 (pdf)

Printed in Sweden by Media-Tryck, Lund University, Lund 2021



Media-Tryck is a Nordic Swan Ecolabel certified provider of printed material. Read more about our environmental work at [www.mediatryck.lu.se](http://www.mediatryck.lu.se)

**MADE IN SWEDEN** 

*Listen...*  
*All this takes a lot of gettin' use to...*  
*And you do get used to it...*  
*After a while...*  
*-Darren Korb*





# Contents

List of publications . . . . .	ii
Acknowledgements . . . . .	iii
Popular summary in English . . . . .	vi
Popular summary in Swedish . . . . .	viii
<b>Introduction</b>	<b>I</b>
1 Nanowire Growth . . . . .	7
2 Monte Carlo Methods . . . . .	11
3 Thermodynamics . . . . .	15
4 Kinetics . . . . .	21
<b>Modeling Nanowire Growth</b>	<b>29</b>
5 Simulation Frameworks . . . . .	31
6 Crystal Structure Selection . . . . .	39
7 Growth Dynamics . . . . .	45
8 Simulating Ternary Nanowire Growth . . . . .	51
9 Concluding Remarks and Outlook . . . . .	57
10 References . . . . .	61
<b>Scientific publications</b>	<b>69</b>
Author contributions . . . . .	69
Paper I: Understanding GaAs Nanowire Growth in the Ag-Au Seed Materials System . . . . .	71
Paper II: Simulation of GaAs Nanowire Growth and Crystal Structure . . . . .	97
Paper III: Effect of Radius on Crystal Structure Selection in III-V Nanowire Growth . . . . .	115
Paper IV: Independent Control of Nucleation and Layer Growth in Nanowires . . . . .	125
Paper V: Simulating Vapor-Liquid-Solid growth of Au-seeded InGaAs Nanowires . . . . .	143

# List of publications

This thesis is based on the following publications, referred to by their Roman numerals:

- I **Understanding GaAs Nanowire Growth in the Ag-Au Seed Materials System**  
E. K. Mårtensson, A. M. Whiticar, M. de la Mata, R. R. Zamani, J. Johansson, J. Nygård, K. A. Dick and J. Bolinsson  
Crystal Growth & Design, 2018, 18, 11, 6702-6712
- II **Simulation of GaAs Nanowire Growth and Crystal Structure**  
E. K. Mårtensson, S. Lehmann, K.A. Dick, J. Johansson  
Nano Letters, 2019, 19, 2, 1197-1203
- III **Effect of Radius on Crystal Structure Selection in III–V Nanowire Growth**  
E. K. Mårtensson, S. Lehmann, K.A. Dick, J. Johansson  
Crystal Growth & Design, 2020, 20, 8, 5373-5379
- IV **Independent Control of Nucleation and Layer Growth in Nanowires**  
C. B. Maliakkal, E. K. Mårtensson, M. Tornberg, D. Jacobsson, A. R. Persson, J. Johansson, R. Wallenberg, K. A. Dick  
ACS Nano, 2020, 14, 4, 3868-3875
- V **Simulating Vapor-Liquid-Solid growth of Au-seeded InGaAs Nanowires**  
E. K. Mårtensson, J. Johansson, K. A. Dick  
Unpublished Manuscript

All papers are reproduced with permission of their respective publishers.

## Acknowledgements

There are many people who, in one way or another, have helped me through this period of my life. There are some people who have earned special mentions, and perhaps none more than my main supervisor, Kimberly. I am amazed at how you manage to combine being a fantastic researcher, a fantastic teacher and a fantastic group leader all at once. I am extremely grateful to have had you as a supervisor throughout the years. Thank you for helping me improve my work by helping me to improve myself. Thank you for providing unyielding support when I needed it. Thank you for teaching me much about what leadership should be. Know that I had not been the researcher I am today without you as my main supervisor.

Jonas. As a co-supervisor, you were in charge of supporting me when it came to the theory of nanowire growth. I started out as an experimentalist but, as is clear when reading this thesis, I ended up abandoning the experimental side of things and doing purely theoretical work instead. This would not have happened if you had not helped in making nanowire growth theory fun. Thank you for all our interactions throughout the years!

Sebastian. As a co-supervisor, you were in charge of supporting me when it came to the experimental side of nanowire growth, and I started out doing mainly experimental work but... Ummm... Anyways... I will sorely miss your company, and our quick-chats-about-a-graph turned hours-long-philosophical-discussions about everything and anything which may or may not be related to that graph. Also, thanks for letting me know exactly how much the very fragile quartz shield cost while I was carrying it for the first time. I'm sure I would have dropped it had I not known how expensive it was.

Sepideh. As my co-supervisor in the beginnings of my PhD, thank you for making me feel welcome and showing me the ropes!

Marcus. You are not my co-supervisor. However, your importance to me and my work have been up there, and definitely made you deserving of some sort of title. Honorary Supervisor? Hmm, maybe... Honorary Samwise Gamgee? Better than any Star Wars references at least... Anyways, the other supervisors have no clue how many incredibly stupid ideas that they did not have to hear, only because I had you to discuss them with first. For all the support and friendship at the university, and all the wine and cheese and games outside the university: Thank you!

Throughout the years I have made many friends at the university and at the department. There are (un)fortunately more of you than can be put into a single acknowledgments sections. Know that if you and I have shared either a board game session, a musical song, fuses, a drink at the (nano)bar, a serious discussion, a not-so-serious discussion, a lunch at the lunch-room, a lunch meeting, a mail-thread about how to get my defense or thesis in

order, or simply a laughter along the way, you have been a part of my journey. For that, I am grateful. It would not have been the same without you.

Also, since I know this is the part of the thesis you will all actually read: I know it is a custom within the department to gather coins and give a gift whenever someone defends his or her thesis. Please don't do this for me. I already have more than I need and it is my memories of my time here that I will bring with me into the future.

There are some groups of people which I would like to give an extra shout-out to. I want to say thank you to all the past and present members of the research group! Though the composition of the group has been in constant change throughout the years, the spirit of the group has always remained. The open atmosphere, where one is always welcome to discuss any topic which comes to mind, without any judgment and with plenty of cakes, has done wonders for both my well-being and my research. Thank you all!

A big thanks to the amazing group of people who goes by the name of Dr. Nano. 11 years now since we were brought together... It's been a great journey, and I am so glad I got to share the it with all of you!

To the group of special people: You are awesome! These years would not have been the same without all of you. Can't wait to share another beer with you in the future, though I'm sorry to say it will not be at *that* place.

Thanks to all roommates I've had throughout the years. Although talks about Majorana fermions still sound like danish to me, each and every one of you has taught me something new about the world! It has been great to have you all close by!

I also want to take the opportunity to thank those who I have had the pleasure of interacting with through my teaching. This goes out to any student who have survived my comments on either a lab report or a master thesis, and to the colleagues who have taught alongside me. I would like to give a special shout out here to the sustainability crew. I has been a wonderfully difficult, wicked and instructive adventure.

To my parents, friends 'on the outside', and to the second-in-commands; thanks for reminding me that there is a world outside of the world of nanowires. And to my brothers; thanks for all the ~~sarcasitic comments~~ support! Remember, no one cares who finished first. 'Who started the trend?', now that's the important question! Well, that and 'Who makes the best bread?'

My dearest, Sara! (With a comma after dearest.) Without you, I would likely have spent more time at work, and it's entirely possible that this thesis would be a tiny bit better as a result. What you have given me instead is much important to me than any thesis could ever be. With you by my side, I am happy. From the bottom of my heart, thank you for everything!

And finally, Malte. It is truly inspiring to see you try something, fail miserably, try again, and repeat that a few thousand times. Then, when you finally succeed, there is only pride and joy in your face having learned a new skill. It is amazing to watch you grow, always in motion and always evolving. Never change!

## Popular summary in English

Gardening is a popular pastime for many people. You carefully plant a tomato seed in the soil, give it some water to reach just the right amount of humidity in the soil for it not to dry out and not to drown. With time, heat, sunlight and more watering you can watch the seed sprout, then grow into a plant. The plant continuously grows and if the leaves start to become singed you can move it to a more shaded spot. If the leaves start to look too pale and yellow, you can add a bit of manure to improve the soil and watch the plant regain its green color. In more cold and cloudy periods, the plant can go for days without watering but if the sun is shining and the thermometer reads  $40^{\circ}\text{C}$  then you probably need to tend to the plant more than once a day. You often want to promote apical dominance, and for growing tomatoes this means removing any new shoots from the axils. If you continuously care for the plant, at the end of the season you can find yourself with some amazingly ripe tomatoes.

Growing nanowires is in many ways similar to growing tomatoes. You start with a seed. This time it is not a millimeter-sized organic grain but a sphere, typically made of gold, with a diameter of maybe 30 nanometers. Instead of soil, you place the seed particle on a substrate which then goes to a growth reactor and not a greenhouse. Using a watering can during nanowire growth is a bad idea. Instead of maintaining a good level of humidity, you precisely control the concentrations of growth precursors (molecules containing for instance gallium or arsenic if you want to form gallium arsenide nanowires) in the vapor above the substrate. If you provide too many precursor molecules to the reactor, or too few, the growth fails. Which level of precursor-concentration is just right depends on the temperature of the reactor, again similar to the growth of the tomato. You want to maintain a high aspect ratio in your nanowire, similarly to promote apical dominance in the tomato plant, which means finding combinations of growth parameters which promote a high axial growth rate and a comparatively low radial growth rate. If you continuously provide the right environment for the seed particle, at the end of the growth session you can find yourself with a perfect array of tall, uniform, semiconducting nanowires.

Throughout the past centuries, people have learned how tomato plants should be treated and passed the information on. The seeds have been refined to find varieties which are best suited for different climates. Growers know which concentrations of nitrogen, phosphorus and potassium are optimal for the soil to have and know exactly which signs to look for if something is off and how to remedy it.

Safe to say, nanowires have not been grown for centuries. Because of their small size, you need powerful electron microscopes to even see that they are there, and these microscopes are typically not compatible with the growth reactor. This means that while a nanowire grower does have full control over the seed, the substrate, the temperature and the precursor

flows, one will only be able to analyze the growth process using the end results. Imagine that you are given a few pictures of withered tomato plants and are asked to give advice to a novice tomato-grower on how to improve for next season.

Because of the difficulties of not being able to see everything that is happening during nanowire growth, I have worked on developing models for simulating the growth using a computer. The focus has been to create models which are as close to real experiments as possible. When I create models, which can generate similar trends as are found experimentally, then I can analyze the simulated data during the growth and find explanations for the experimental trends.

When we understand something, we have much more control over it. My hope is that the explanations that I have helped bring to the research community will aid those doing the experimental work when they are adapting their growth recipes to achieve specific goals. I also hope that the modeling frameworks and thought processes can inspire those interested in the modeling itself.



## Popular summary in Swedish

Grönsaksodling är ett populärt tidsfördriv för många människor. Man planterar försiktigt ett tomatfrö i jorden, ger det lite vatten för att nå precis rätt mängd fukt för att det inte ska torka ut och inte drunkna. Med tid, värme, solljus och mer vattning kan man se hur fröet gror och sedan växer till en planta. Tomatplantan växer kontinuerligt och om bladen börjar se lite brända ut kan man flytta den till en mer skuggig plats. Om bladen börjar se bleka och gula ut kan man lägga till lite gödsel för att förbättra jorden och se hur växten återfår sin gröna färg. I mer kalla och molniga perioder kan plantan klara sig flera dagar utan att bli vattnad, men om solen skiner och termometern visar 40 °C måste man förmodligen se efter plantan mer än en gång om dagen. Man vill ofta främja den apikala dominansen i tomatplantorna, och det innebär att man hindrar den radiella växten genom att ta bort nya skott som växer mellan stammen och grenarna. Om man ständigt tar hand om växten kan man i slutet av säsongen ha en skörd av smakrika, solmogna tomater.

Nanotrådväxt liknar på många sätt tomatodling. Man börjar med ett frö. Den här gången är det inte ett organiskt korn i millimeterstorlek utan en sfär, vanligtvis bestående av guld, med en diameter på kanske 30 nanometer. I stället för jord placerar man fröpartiklarna på ett substrat som sedan går till en tillväxtreaktor och inte ett växthus. Att använda en vattenkanna i nanotrådväxt är en dålig idé. I stället för att upprätthålla en god luftfuktighet styr man växten genom att kontrollera koncentrationerna av metal-organiska föreningar (om man vill växa nanotrådar av galliumarsenid så är detta molekyler som innehåller antingen gallium eller arsenik). Om man tillsätter dessa föreningar i alltför hög koncentration, eller för låg koncentration, så kommer växten att misslyckas. Vilken koncentration som är precis rätt beror på temperaturen i reaktorn, vilket återigen speglar tomatodlingen. Man vill behålla en hög aspekt-ratio i dina nanotrådar, liknande att främja apikal dominans i tomatodlingen, vilket kräver att man hittar kombinationer av tillväxtparametrar som främjar en snabb axiell tillväxt och samtidigt ger en relativt långsam radiell tillväxt. Men, om man kontinuerligt tillhandahåller rätt miljö för fröpartiklarna kan man i slutet av tillväxtpasset hitta ett perfekt uniforma halvledande nanotrådar i ett mönster på substratet.

Under de senaste århundradena har människor lärt sig hur tomatplantor ska behandlas, och fört informationen vidare i generation efter generation. Fröna har förädlats för att få sorter som är bäst lämpade för olika klimat. Odlarna vet vilka halter av kväve, fosfor och kalium som är optimala för jorden och vet exakt vilka tecken man ska leta efter för att se om något är fel och hur man kan åtgärda det.

Man kan med säkerhet säga att nanotrådar inte har odlats i århundraden. Eftersom nanotrådar är just trådar i en storlek som bäst uttrycks i nanometer behöver man kraftfulla elektronmikroskop för att ens se att de finns där, och dessa mikroskop är vanligtvis inte kompatibla med reaktorn som används för att växa trådarna. Detta innebär att, trots att en

nanotråds-växare har full kontroll över den initiala fröpartikeln, substratet, temperaturen och koncentrationerna av de metal-organiska molekylerna, kommer man bara att kunna analysera tillväxtprocessen med hjälp av slutresultaten. Detta är många om mycket som att få några bilder av vissna tomatplantor, tagna flera månader efter att säsongen är över, och med hjälp av dem ge råd till en nybörjare inom området om hur hen kan förbättra odlingen till nästa år.

På grund av denna problematik, att inte kunna ha information om allt som händer under nanotrådstillväxt när det faktiskt händer, har jag arbetat med att utveckla modeller för att kunna simulera nanotrådsväxt med hjälp av en dator. Fokus har varit att skapa modeller som är så nära verkliga experiment som möjligt. När modellerna kan generera liknande trender som ses i experimentella data, betyder det att man kan analysera den data som genererats under simuleringen för att bättre förstå vad som händer i den experimentella växten.

När vi förstår något har vi mycket mer kontroll över det. Jag hoppas att förklaringarna bakom olika växttrender som jag har undersökt kan komma att hjälpa de som växer nanotrådar experimentellt att optimera sina växtrecept för att uppnå det som de vill uppnå. Jag hoppas också att de teoretiska ramverk som jag skapar, och idéerna bakom dem, kan vara till inspiration för de som är intresserade av att bygga vidare på modellerna.



# Introduction

*How do I want to do this?*  
*-Matthew Mercer (2:87)*

There has been a growing interest in semiconducting III-V nanowires throughout the last decades. While a III-V nanowire is nothing more than a crystalline piece of III-V material in a thin, long shape; this particular shape does offer some significant benefits to devices. Simply due to its shape, there is interest in using nanowire arrays as building blocks for solar cells due to the increased harnessing capabilities provided by the resonance absorption of light<sup>1,2</sup>. In electronics, nanowire transistors have great potential, since they can have the gate all around the semiconductor which is a great geometry for a transistor<sup>3</sup>. In betavoltaics, the nanowires can be completely immersed in radioactive material, which can improve the efficiency of the electron-hole pair generation due to a higher fraction of the isotropic radioactive decay which reach the active regions of the nanowires<sup>4</sup>. These examples are shown in Figure 1. While no one knows what the fall out of the current nanowire research will be, there is high hope that some of these prospects will brighten our common future.

These benefits are based on the geometry of the nanowires and are thus independent of the fabrication process. The fabrication of nanowires can be done in one of two ways. One is referred to as the bottom up approach and the other as the top down approach, see Figure 2a,b. In the bottom up approach, the structure is assembled on top of a bare substrate, whereas the top down approach is conceptually the same as the sculpting of a statue. One starts with a big slab of material and then selectively removes bits and pieces until the desired structure is reached. While there are no nanoscale chisels or hammers, various forms of lithography operate at these low dimensions. With lithography techniques the nanowires are formed by masking areas of the sample, followed by anisotropic etching of the uncovered areas. While this method can be efficient, it has the innate downside that you cannot form a nanowire of a certain material unless you can grow the bulk version of it, and bulk materials are notoriously bad at accommodating strain.

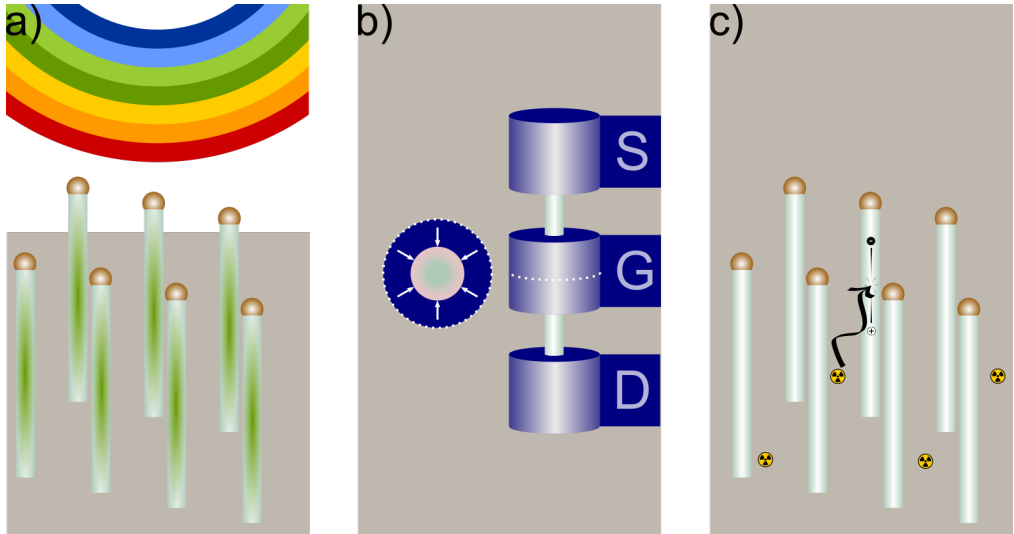
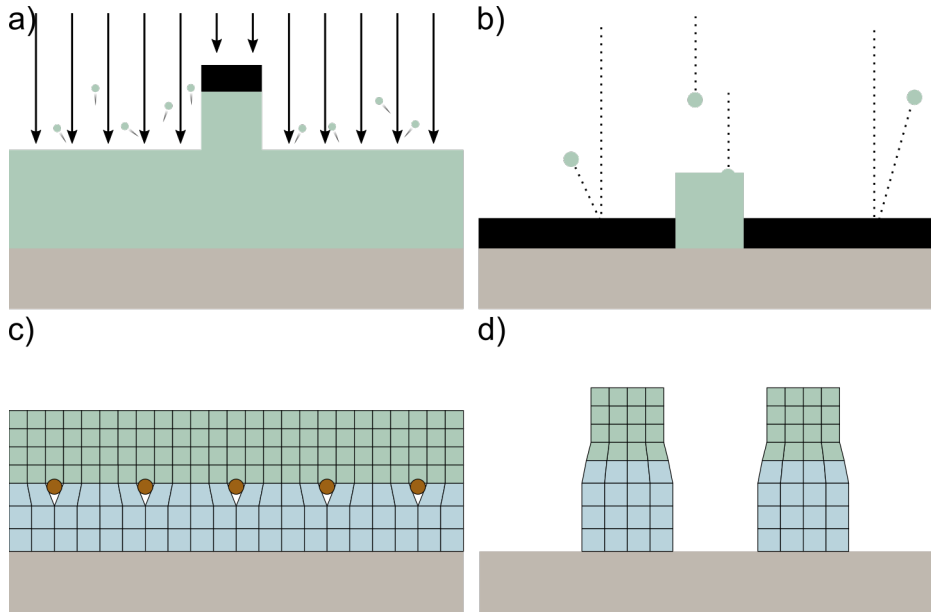


Figure 1: Schematic figures of a nanowire array absorbing incoming light (a), a nanowire field effect transistor with a wrap around gate (b), and nanowires surrounded by radioactive material for betavoltaic applications (c).

Epitaxy is a bottom up approach wherein a crystalline material is grown in an orderly fashion on top of a substrate. The substrate can be of the same material as the top material, this would be referred to as homoepitaxy, or of a different material, referred to as heteroepitaxy. In heteroepitaxy, strain can become a significant issue if the lattice parameters of the two materials differ significantly from each other, as the epitaxial growth of a mismatched heterostructure forces the top layer material to adapt to the size of the substrate material. If the top material has a smaller lattice parameter, it will be stretched out in the plane of the interface and can only relax this deformation in the growth direction. Typical in this growth scenario is that the first few layers will be strained, but remain defect free. However as the growth continues, the total energy contribution due to the strain will increase with each layer until at one point it will become energetically favorable to create defects at the interface between the two materials. When the defects have formed, the top layer no longer needs to perfectly align with the bottom layer, and the system becomes relaxed. This is shown in Figure 2c. Defects can significantly deteriorate the performance of the material<sup>5</sup>, which is why lattice matching is so important in large area growth.

In nanowires, the small dimensionality allows for alternative means of relaxing strain<sup>6</sup>. If one considers the same heterostructure in a nanowire, the interface is limited to the cross-section of the nanowire. In the radial directions, the nanowire is free to change its shape, and this means that the nanowire can gradually widen or narrow its diameter and thereby relax its strain as it grows taller. This can be seen in Figure 2d. To take advantage of this radial relaxation, the nanowire must be formed using the bottom up approach. Here, the process starts with a bare substrate, and material is then added to selective parts of the



**Figure 2:** Schematic figures of nanowire formation using the top down approach (a) or the bottom up approach (b), and heterostructures with mismatched materials in a thin film configuration with defects (c) and in a relaxed nanowire shape (d). The brown dots represent defects, and the size of the pattern represents the size of the respective lattice.

substrate to form the nanowires. The selectivity in the growth can come from e.g. masking parts of the sample using lithography techniques as is shown in Figure 2b.

This ability to relax the strain radially gives nanowires formed using the bottom up approach a lot of potential, for instance when it comes to opto-electronic applications. In tandem solar cells, the idea is to grow different singular solar cells on top of each other, with different band gaps, to increase the efficiency of the device. For bulk systems, the decision of which material combination to use is typically determined by lattice matching. This gives little room to maximize the theoretical efficiency of the final device. Even mismatches as low as 0.08% have been reported to lead to device-deteriorating misfit dislocations in tandem solar cells<sup>7</sup>. In nanowires, dislocation-free heterostructures of GaAs-GaSb have been grown<sup>8</sup>, which has a mismatch of around 10%. This ability to relax the strain radially, can enable one to choose material combinations based on the potential device performance to a larger extent. This could apply to growing tandem solar cells at theoretically optimized band gaps<sup>9</sup>, or as a route to make InGaN quantum wells in GaN<sup>10</sup> which could cover the entire spectrum for light emitting diodes.

Grown III-V nanowires can in addition to the stable zinc blende (ZB) crystal structure also form the metastable wurtzite (WZ) structure<sup>11</sup> (or inversely for nitrides, where WZ is stable, segments of ZB can form<sup>12</sup>). The polytypism in nanowire growth will be discussed in detail throughout the thesis, and it is of interest as the crystal structure can alter the

properties of the semiconductor in beneficial ways. For instance; ZB has a conduction band offset with respect to WZ in the InAs materials system. As a result, a ZB InAs nanowire with a thin WZ segment in the middle has a tunnel barrier in the conduction band<sup>13</sup>. For GaP, the band gap is indirect in the ZB phase, but for the WZ phase it has been shown to be direct<sup>14</sup>, which is highly relevant for its potential use in opto-electronic devices.

In order to take advantage of all benefits offered by the III-V nanowires, the bottom up approach must be used; however, the ability to grow heavily mismatched defect free heterostructures in a metastable crystal structure is not only a blessing when it comes to nanowire growth. Having two different crystal structures often leads to nanowires with an unwanted mixed structure, or individual stacking faults embedded into the otherwise homogeneous nanowire<sup>15</sup>. While it is possible to grow nanowires with a heterostructure of different materials<sup>16,17</sup> or dopants<sup>18</sup>, abrupt junctions are difficult to achieve. Nanowire growth is conventionally catalyzed by a so-called seed particle, and the choice of material for this seed particle affects the growth<sup>19,20</sup>, adding another layer of complexity to the process. In addition, these aspects often need to be addressed simultaneously, which is difficult since they are not necessarily independent of each other. An example of this is that the addition of dopants during growth have been shown to affect the crystal structure of the growing nanowire<sup>21,22,23</sup>. A very high level of experience, control and understanding is crucial to successfully grow the desired end structures.

Typically, the understanding of nanowire growth has been severely limited by the fact that the design of the reactor used to grow nanowires does not allow one to observe the growth while it happens. One has historically been left with pre- and post-growth analysis to try and extrapolate what occurred during the actual growth. Due to this lack of real time data, and the complexity of the process, it is difficult to draw conclusions on the correlation between the fundamental aspects governing the growth and the experimentally accessible parameters. This difficulty to transfer knowledge from the experimental growth to the fundamental theory works both ways, and because of this I would argue that novel nanowire structure are typically found through experimental trial-and-error, combined with the experience of the experimentalists. Growth theory is typically used to explain experimental results after the fact, and is seldom used in a predictive manner which can guide the experimentalists in their pursuit. But it could be.

My research has focused on improving the theoretical modeling of nanowire growth, and finding new ways to correlate theory and experiments. The main contributions have come through the development of simulation frameworks, where the inputs and outputs of the simulations correspond to the inputs of experimental growth and the outputs of the post-growth observables. This has led to five original works, around which this thesis is built. The five papers are summarized as follows.

In Paper I, I examined the growth of GaAs nanowires using three different Au-Ag alloys

as the seed particle material. Here, I used thermodynamics to understand pieces of the growth process, by combining an analysis of the chemical potential of Ga in the different seed materials with experimental bottom up growth. The usage of different seed particle materials allowed the probing of how the growth differs, and is similar, for the different seed materials. Here, I used thermodynamics to compare the chemical potential of Ga in the different seed materials based on the experimental post-growth analysis.

In Paper II, I presented the first iteration of the Monte Carlo framework I use to simulate the growth of nanowires. The understanding of the thermodynamics of the materials system was here combined with mass transport, classical nucleation theory and a hit-and-miss Monte Carlo approach. This resulted in a framework which allows one to vary the mass flows of growth species, and simulate the evolution of the seed particle as well as the nucleation new layers in the nanowire. Here, it was used to specifically evaluate how the flow of As can affect the crystal structure selection in Au seeded GaAs growth. Experimental trends were theoretically reproduced, and data from the simulation was analyzed to provide explanations for the underlying governing effects.

In Paper III, I continued working on the model of Paper II by incorporating substrate diffusion and the Gibbs Thomson effect into the model. These aspects of nanowire growth are well known to be connected to the size of the nanowire, and allowed the evaluation of how the radius can affect the crystal structure selection in Au seeded GaAs growth. We found that the surface to volume ratio is important for nanometer sized objects, and explained how this geometrical consideration can affect the dynamics of the simulations to promote either the WZ phase or the ZB phase during growth.

In Paper IV, I worked together with colleagues who use a state of the art combined in-situ transmission electron microscopy and metal-organic vapor phase epitaxy machine at the National Center for High-Resolution Electron Microscopy (nCHREM) in Lund. They grew Au-seeded GaAs inside the microscope and we analyzed the two distinct periods which make up the nanowire growth cycle, the incubation period and the layer propagation period. Here, I adapted the model to not only include the nucleation (connected to the incubation), but to also allow for modeling of the layer propagation by incorporating droplet depletion into the framework. The modeling allowed us to understand the experimental results, and also to understand a wider parameter space than was possible to test experimentally.

Next, in Paper V, I gave the model an overhaul to be able to model a non-binary III-V growth. In this paper, I stepped away from using the classical nucleation theory, and instead handled nucleation and layer propagation through the attachment and detachment of individual III-V pairs. With this new framework, I could study how the solid composition varies throughout the growth of each bilayer, and how this can help us understand the ternary growth process.



To frame the contents of these papers, and help introduce the reader into my interdisciplinary field of research, this thesis will be organized into two parts. The first part is meant to be a general description of what I consider to be key areas of the thesis and/or the field, and consists of the following sections.

In section 1, I give a description of experimental growth of nanowires. I focus on particle assisted growth using the metal-organic vapor phase epitaxy technique.

In section 2, I give a presentation of Monte Carlo methods. Here I describe how random numbers can be applied to solve problems, sample from distributions, and help us understand both deterministic and non-deterministic processes.

In section 3, a fundamental description of the thermodynamic framework is presented and described. This covers how the world can be described solely from the perspective of bulk energies, and how this can be applied to find equilibrium.

In section 4, a description of nucleation kinetics is presented. Here, the framework leading up to the Classical Nucleation Theory is presented, starting from the Becker-Döring rate equations. This describes the initial clustering of monomers, and their transition from unstable and decaying, to stable and growing nuclei.

In the second part, I will present how I have applied the knowledge from these key areas on the field of nanowire growth modeling. The second part is divided into the following sections.

In section 5 I present my different approaches for simulating nanowire growth, and discuss their similarities and differences.

In section 6, the topic of crystal structure selection in nanowire growth is covered. I give a presentation on the history of the field, and touch on the work in Paper I and discuss the results of Papers II- III.

In section 7 I focus on what the simulations reveal in relation to the dynamics of nanowire growth, and general responses to changes in precursor flows. Here I discuss how the flows can affect the composition in the seed particle, as well as the dynamics of the nucleation and the step propagation periods from Paper IV.

In section 8, I discuss my simulations on the growth of InGaAs nanowires. This focuses on the thermodynamics of the As-Au-Ga-In materials system, the growth of heterostructures, and the steady state growth discussed in Paper V.

In section 9, I bring up some remarks upon the conclusion of my time as a Ph.D. student, discuss the impact of my work on society, and present an outlook of my work. I discuss the current state of the models, what they could be and the gap between those two.

# I Nanowire Growth

In theory, I have done a lot of work. However, I have also been on the experimental side of nanowire growth. The main reason for developing the simulation models was to bridge the gap between existing theory and the experimental growth of nanowires, in order to provide guidance when developing growth recipes. For this reason, it is important to explain how nanowires are typically grown, and what information can be gained from the growth. It is also highly important to have an understanding of the experimental growth in order to understand the limitations of the simulation frameworks, since they simply cannot take all aspects of experimental growth into consideration. While there are many ways to grow nanowires, the one which I have used and will describe is particle-assisted growth in a metal-organic vapor phase epitaxy (MOVPE) setup.

## I.1 MOVPE Reactor

MOVPE is a technique to deposit growth species, slowly and with a high level of control, which enables epitaxial growth of the desired material at a specific location. The design of these MOVPE reactors may vary, but here I will give an introduction to the system which I have used in Paper 1. The growth chamber, where the actual deposition of materials takes place, is schematically shown in Figure 3a.

The growth chamber consists of a rotating susceptor made of an inert material, on which the sample is placed. Within the susceptor there is a heating coil, which can locally heat it and the sample to the desired growth temperature. This is important since the deposition of growth materials requires an elevated temperature. During growth, growth species in the form of precursor molecules are supplied to the surrounding vapor phase via a showerhead above the susceptor. For Ga, this would be tri-methyl-gallium (TMG) or tri-ethyl-gallium

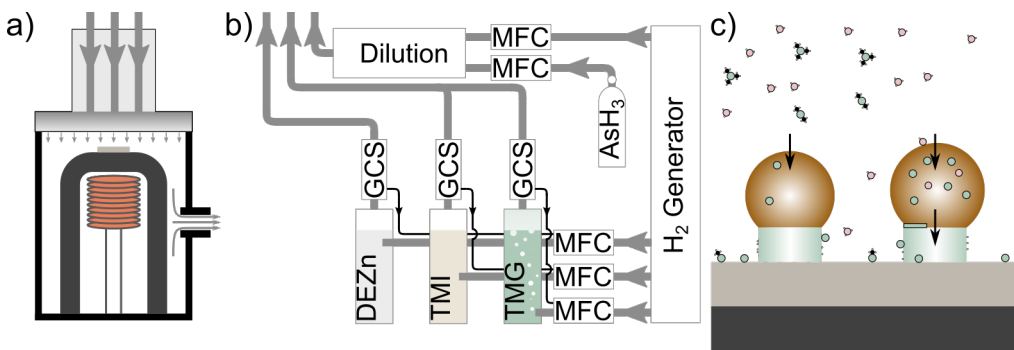


Figure 3: Schematic illustrations of the reactor chamber of an MOVPE machine (a), the gas handling system (b), and a sample with growing nanowires (c).

(TEG), for As this would be tert-butyl-arsenic (TBAs) or Arsine ( $\text{AsH}_3$ ). A reason for using precursors is that they, in contrast to their pure elemental form, are volatile and can be vaporized, with a high level of control, and transported away using a carrier gas. The precursors then decompose when exposed to the heat of the susceptor, leaving the growth species behind while the gaseous by-products flow with the carrier gas towards the exhaust. This means that as long as one can control the concentrations of precursors in the vapor phase, and the temperature of the susceptor, one can control the deposition rate of growth species to the sample.

While this sounds straight forward, the pyrolysis process is complex. Taking TMG as an example: if TMG is kept at elevated temperatures one could expect the gas to contain a mixture of TMG, di-methyl-gallium, mono-methyl-gallium, H,  $\text{H}_2$ ,  $\text{CH}_4$ ,  $\text{C}_2\text{H}_2$ ,  $\text{C}_2\text{H}_4$ ,  $\text{C}_2\text{H}_6$ , with a composition that depends on time and temperature<sup>24</sup>. The overall reaction rates have been shown to depend on the carrier gas used<sup>25</sup>, the concentration of other precursors such as Arsine<sup>26</sup> as well as on which surfaces are available in the reactor<sup>26,27</sup>.

Despite this complexity, if one can maintain a steady flow of precursors, with a constant gas phase composition, then the growth can be extremely stable. The precursors are supplied from the gas-handling system (GHS). The GHS, shown schematically in Figure 3b, consists of three separate lines which connect to the showerhead of the growth chamber, and the different lines supply group V, group III and dopant precursors, respectively.

Metal-organic sources are extracted using so called bubblers. Using Ga as an example: a bottle of liquid TMG is kept in a water bath with an immersion circulator to maintain a constant temperature. An inlet for hydrogen carrier gas is situated under the liquid inside the TMG bottle, and the outlet is placed above the liquid TMG. To extract TMG to the growth chamber, a mass flow controller (MFC) injects the desired flow of  $\text{H}_2$  into the bubbler. As the  $\text{H}_2$  bubbles through the bottle, it becomes saturated with TMG molecules at a concentration which depends on the temperature of the bubbler and the pressure inside the bottle. The saturated gas then passes through a gas concentration sensor (GCS), which measures the concentration of TMG in the outlet. The GCS can increase or decrease the MFC settings to ensure that the concentration remains constant throughout the growth, but importantly also to ensure that the growth is reproducible over time.

Arsine is a special case, since the hydride is gaseous at room temperature. Therefore, an MFC is sufficient to extract a controlled flow of arsine. To be able to utilize a wider range of flows than what is allowed by the MFCs, the setup contains a dilution chamber. Here, one part arsine can be diluted with 99 parts  $\text{H}_2$ , and then a part of that mixture can be injected into the growth chamber. This enables growth with both high and extremely low flows of arsine.

With an understanding of how the growth species are transferred to the sample, it is now time to look towards the sample itself.

## 1.2 Gold Seeded Nanowire Growth

Growth of nanowire-like structures (albeit at a  $\mu\text{m}$  scale) was described in literature already back in 1964<sup>28</sup>, and they were a result of unintentional growth with Au seeds using the vapor-liquid-solid (VLS) method. Today, more than half a century later, Au-seeded VLS growth is still one of the most widely used growth methods. As shown in Figure 3c, this is based on the net transfer of growth material from a vapor to a liquid phase, and from a liquid to a solid phase. The vapor phase consists of the carrier gas flowing through the MOVPE reactor, which contains a certain concentration of the desired precursors. The growth species travel to the Au particles, which in VLS growth are in the liquid phase. Pure Au is not liquid at typical nanowire growth temperatures (between  $400^\circ\text{C}$  and  $600^\circ\text{C}$ ). However, alloying Au with growth materials such as Ga or In can dramatically reduce the melting temperature of the particles below the growth temperatures. From the liquid phase, the growth species then transform to the solid phase which is the actual nanowires.

Before the growth starts, the sample needs to be prepared with the desired seed particles. To get the particles on the sample, one of three approaches is typically used; thin film annealing, direct particle deposition, or lithography patterning<sup>29</sup>. In thin film annealing a thin layer of the seed material, typically with a thickness of a few  $\text{\AA}$ , is deposited uniformly on top of the substrate. Upon annealing at high temperatures the material in the layer reorganizes into particles. This has the benefit of being a very simple and clean approach since the only pre-processing step is the thin film deposition. The downside is that particles have a large spread in size, and are formed randomly spaced on the sample. With direct particle deposition, pre-generated particles with the desired size are deposited on the sample via e.g. an aerosol-system or a colloidal solution. This yields particles with a narrow size distribution, but still randomly placed. This method ranges from being moderately expensive and very clean when using an aerosol system to being very inexpensive and having a high risk of contamination when using a colloidal solution. The last approach is the lithography-defined particles. Here, the substrate is typically coated with a resist, which is then patterned by a lithography processes, e.g. electron beam lithography. This leaves particle-sized holes in the resist, at user-defined positions on the sample. After depositing a layer of the seed material on the entire sample, the resist is removed along with any material sitting on top of it. This finally results in particles with size control, density control and positional control, but requires more processes which runs a high risk of contaminating the sample and is much more labor and equipment intensive than the alternatives.

Regardless of which approach was used to deposit the seed particles on the sample, the next step is to grow the actual nanowires. An example of a growth recipe for a Au-seeded WZ-ZB GaAs heterostructure is shown in Figure 4, together with some schematic snapshots of a single wire at different timestamps. The growth typically starts by ramping up the temperature to perform an anneal. This is done mainly to remove any native oxides on the surface

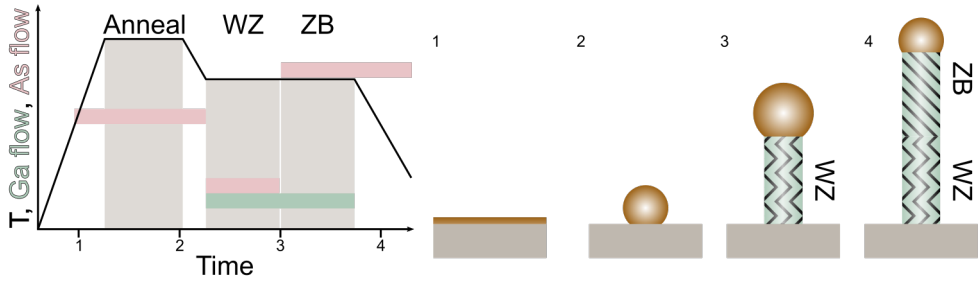


**Figure 4:** A schematic representation of a typical GaAs nanowire recipe using MOVPE, together with schematic figures of the growing nanowire throughout the process

of the substrate<sup>30,31</sup>, and to dewet any thin film of Au into particles. A background flow of  $\text{AsH}_3$  is used to minimize any degradation of the surface of the sample<sup>32</sup> and counteract the non-congruent evaporation<sup>33</sup>. Next, the temperature of the susceptor is reduced to the desired growth temperature and, after it has stabilized, a flow of TMG is introduced and the flow of  $\text{AsH}_3$  is reduced to grow the WZ base of the nanowire. After sufficient time has passed, the flow of  $\text{AsH}_3$  is increased to grow a ZB top segment for the nanowire<sup>34</sup>. Next, the temperature is slowly reduced in preparation to open the reactor and take the sample out. During this cooldown the Ga flow is always turned off, but the arsenic source is often left on. The main purpose of this is to reduce any decomposition of the nanowire, either on the sidewalls of the nanowire or via the liquid-solid interface<sup>35</sup>; but this can also lead to some continued growth during the cooldown process which depletes some of the Ga from the seed<sup>36,37</sup>.

This marks the end of the nanowire growth, and the sample can be taken out for post-growth analysis or device fabrication. Obviously, this is just one example of a nanowire growth recipe. The outcome can be changed by varying the substrate, the particle size and distribution, the temperature(s), times, flows, precursors, growth species, and so on; but this section has outlined a general growth procedure and the typical toolbox of an experimental nanowire grower.

## 2 Monte Carlo Methods

In this thesis I, like many others, define Monte Carlo (MC) methods as any methods which relies on random numbers as part of their routines. This is obviously a very broad definition, but this broadness is also reflected in the wide variety of uses for the MC methods. It can find uses in basically all fields of science, and is often in association with tasks which are not deterministic in nature. Since non-deterministic processes can not be analyzed directly, and are typically described as random, they often make excellent candidates for MC methods. That being said, the perhaps most straight forward example of an MC method is integration, which is definitely deterministic. While analytical methods can struggle with non-deterministic processes, MC methods have no issues with deterministic processes.

While many functions are simple to integrate numerically other functions can be basically impossible, especially when the integration is in many dimensions. Intuitively, it may seem that random numbers can do little to the case of integration, but here an example of just that will be presented. The example is to integrate the equation of a circle with a radius of 1 in the first quadrant:

$$f(x) = \sqrt{1 - x^2}, \quad \int_0^1 f(x) dx = \frac{\pi}{4} \quad (1)$$

The integral in this case is known to be  $\pi/4$ , a quarter of the area of a circle. To find the integral using random numbers, a nice and easy help function is utilized,  $g(x)$ . The only requirement of this function is that it should be greater than, or equal to, the real function  $f(x)$ , and that it can be easily integrated. For this example, the uniform  $g(x) = 1$  is used, and in the given interval, its integral is 1. Since  $f(x) \leq g(x)$ , the integral of  $f(x)$  must be some fraction of  $\int_0^1 g(x) dx = 1$ . To find this fraction, random numbers are used. Conceptually, this is shown in Figure 5

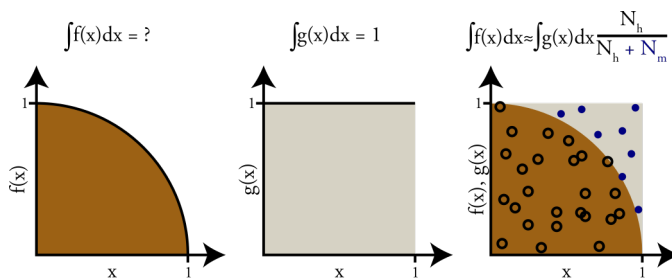


Figure 5: Graphs of the equation of a circle, the help function, and the two functions together. The symbols in the rightmost graph represent hits (black rings) and misses (blue circles).

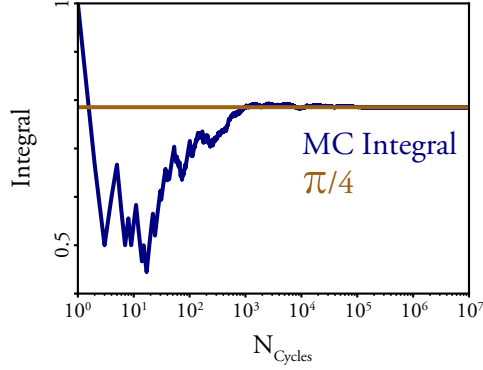


Figure 6: Graph showing how the accuracy of the MC integration scales with the number of cycles.

The fraction can be found using the hit-or-miss method for a number of cycles. In each cycle, a random value for  $x$  is generated according to the  $g(x)$  function, which in this case means  $x_n = U$ . This  $U$  represents a random number between 0 and 1, generated from a uniform distribution. This is the 'standard unit' when it comes to generating random numbers. Whenever there is a need for sampling from a different distribution, as will be covered later in this section, a uniform random number  $U$  is generated, and then converted to the desired distribution using some function.

Now, once an  $x_n$ -value is generated, a  $y_n$ -value is generated according to  $y_n = U_2 g(x_n) = U_2$ , where  $U_2$  is another random number. Now it is time to compare this generated  $x_n, y_n$  pair to the real function. If  $f(x_n) \geq y_n$ , then the generated pair is considered a hit (i.e. it falls under the  $f(x)$ -curve). If not, it is considered a miss. By repeating this process, and keeping track of the number of hits ( $N_h$ ) and misses ( $N_m$ ), the integral of  $f(x)$  can be calculated:

$$\int_0^1 f(x) dx \approx \int_0^1 g(x) dx \frac{N_h}{N_h + N_m} \quad (2)$$

The result of this integration is shown in Figure 6. As the number of cycles (i.e.  $N_h + N_m$ ) increases, the approximation converges towards the real answer. This gives an example of how random numbers can integrate a function. While MC integration may seem far away from the field of nanowire growth, it does showcase the general hit or miss approach which will be used later.

Now I would like to move on to another quite different, but also relevant, example of how random numbers can be used. This time, the example topic is sample-photon interactions used for medical imaging. As a photon travels through a sample it has a chance to scatter,

transferring some amount of energy to the sample and changing direction. The photon can also transfer all its energy and be absorbed, and potentially produce an electron-positron pair. As a photon travels through a sample, it is not possible to know which type of event will be the next to occur, nor when or where it will happen. This can not be calculated in a deterministic fashion. However, one can calculate the probabilities of each of these events being next if the average rates at which they occur are known. Then, it is possible to use MC sampling to select the next event, and where it will occur, based on these probabilities and averaged rates. For more details regarding this example, the reader is referred to Ref. 38. If there are three possible, uncorrelated, events which happen at average rates of  $R_1$ ,  $R_2$ ,  $R_3$ , with a combined rate of  $R_\Sigma$  then the next event can be sampled. The probability that the next event is of type  $i$  is simply given by  $R_i/R_\Sigma$ , but to find the time of the next event, the probability density function (PDF) needs to be evaluated. The PDF for an exponentially distributed event to happen in a small timestep  $dt$  around time  $t$  is given by Eq. 3.

$$f(t)dt = R_\Sigma \exp(-R_\Sigma t)dt \quad (3)$$

Integrating this PDF yields the probability that no event has happened at time  $t$ :

$$c(t) = \int_0^t R_\Sigma \exp(-R_\Sigma t') dt' = 1 - \exp(-R_\Sigma t) \quad (4)$$

The cumulative probability density function,  $c(t)$ , is a function between 0 and 1 which describes the probability of when an event happens. By replacing this function with a random number from a uniform distribution  $U$  and solving for  $t$ , one can sample a time for the next event from this distribution:

$$U = 1 - \exp(-R_\Sigma t) \Leftrightarrow t = -\frac{\ln(1 - U)}{R_\Sigma} = -\frac{\ln(U)}{R_\Sigma} \quad (5)$$

In the last step, we use the fact that if  $U$  is a random number from a uniform distribution between 0 and 1, then  $1-U$  is also a random number from a uniform distribution between 0 and 1.

With these equations it is possible to generate new events until the complete trajectory of a single photon is known as is shown in Figure 7a. Unfortunately, having a single generated trajectory is completely irrelevant, as it is just one of infinitely many paths that an actual photon may take. That being said, when the process is repeated and several trajectories are generated and viewed as an ensemble, patterns can start to emerge. In Figure 7b, the absorption positions of 1000 photons are shown, and this information can be used to draw



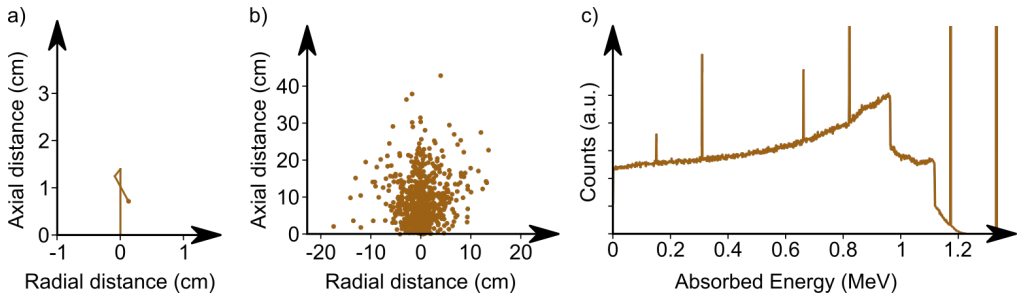


Figure 7: MC simulations of photon trajectories. The trajectory of a single 1 MeV photon in a NaI slab is shown in (a), the absorption positions of 1000 such photons are shown in (b), and the absorption spectrum for a 3x3" NaI detector from 10 million photons from  $^{60}\text{Co}$  decay. The peaks in (c) originate from complete absorption, as well as single and double escapes from pair production.

conclusions regarding the spatial distribution of the absorption. The next step is to simulate data which can be matched against experimental measurements. This is done by simulating the energy absorbed from photons with energies corresponding to the decay of  $^{60}\text{Co}$ , and the geometry of an actual NaI detector. The result for 10 million photons is presented in Figure 7c.

This exemplifies the processes and potential of MC simulations. Knowledge of individual rates or distributions can be used to simulate events, one at the time, which on their own are irrelevant. Over time, these singular events start to show patterns, trends and behaviors which can be analyzed and can provide insights to the process. Finally, by carefully framing the simulations, one can obtain an output which can be directly compared to experimental results. Because everything about the simulation is completely known, this allows one to examine the correlation between the inputs and the output.

### 3 Thermodynamics

Whenever there is a bulk system, consisting of one or more chemical components at a given temperature and pressure, the preferred arrangement of the atoms is determined by thermodynamics. At high temperatures, where the atoms vibrate intensely, the atoms tend to favor the gaseous phase where the distance between the atoms (or molecules) is long. At intermediate temperatures, the atomic vibrations are in balance with the interatomic potentials, and the liquid phase tends to be favored. When the temperature becomes low enough, the atoms tend to arrange themselves into one of the many crystalline phases, favoring the energetic gain of atomic bonds to that of vibrational freedom. There are 230 so called space groups, which describe the distinct symmetries in a particular crystal structure. In the VLS growth of nanowires, the goal is to manipulate the system in such a way that the growth species transform from a gaseous phase to the liquid phase of the seed particle, and subsequently transform from the liquid phase to a specific solid phase. Thus, a solid understanding of thermodynamics is highly important to explain both the fine details as well as the broader strokes of nanowire growth.

The thermodynamic framework gives the ability to understand which phase is favored by a particular system through the means of energy minimization. To find the phase (or combination of phases) which minimizes the energy of the system, there must be a way to describe the energy for each of the relevant phases. In the simplest cases, e.g. a stoichiometric solid, the energy is well described as a function of temperature alone. It should be noted that for the purpose of this thesis the influence of pressure will be neglected, which is reasonable when working with condensed phases. Typically, the energy function can look like<sup>39,40</sup>:

$$g_i^p = a + bT + cT \ln(T) + dT^2 + eT^3 + fT^{-1} + gT^7 + hT^{-9} \quad (6)$$

Here, the molar energy of element  $i$  in phase  $p$ ,  $g_i^p$ , is calculated using variables  $a - h$  which can be found experimentally. The numerical value for  $g_i^p$  gives the energy of the system relative to a corresponding reference system. The absolute value for the energy of a phase is irrelevant, only the difference in energy between two phases has a meaning. Therefore, to have a consistent framework, each element has a defined reference state, the Stable Element Reference (SER), which is the lowest energy state at room temperature and atmospheric pressure. For any other state, the calculated energy is the difference between the current state and the SER energy.

When phases consist of several elements, and are non-stoichiometric, the energy expression becomes more tedious. This describes the liquid phase, which is of interest for describing the energies involved in nanowire growth. The energy,  $g_{mix}^p$ , of such a mixture can be described as:

$$g_{mix}^p = \sum_i X_i g_i^p + RT \sum_i X_i \ln(X_i) + \sum_i \sum_{j>i} E g_{ij} + \sum_i \sum_{j>i} \sum_{k>j} E g_{i,j,k} + \dots \quad (7)$$

The first term sums up the energy contributions of each element as if it was in a pure phase using Equation 6, weighted by the relative molar fractions. The next term takes the entropy of mixing into account, and these first two sums represent the ideal solution model. Next is a summation over all unique pairs of elements in the mixture, and the excess energy of mixing these two elements specifically. The energy of an atom of element A will change depending on if it is surrounded by another atom A, or an atom B. This effect is accounted for by the binary excess energy. Similar terms exist for higher order systems as well, but in terms of actual use, ternary interactions are typically the limit. The excess energy due to the specific mixture of 4 elements, which is not covered by the 6 binary and the 4 ternary excess terms, tends to be negligible.

The excess energy terms are commonly expressed using a Redlich-Kister polynomial. For binaries, this would be:

$$E g_{i,j} = X_i X_j \sum_{v=0}^2 {}^v L_{i,j}(T) (X_i - X_j)^v \quad (8)$$

Here,  ${}^v L_{i,j}$  are called the binary interaction parameters. If one is lucky, these can be found in reported thermodynamic assessments. These are typically the end result of multiple experimental measurements, followed by a fitting procedure to match the theoretical curves to the experimental curves. It should be noted that when  $v$  is even, the terms in the sum are symmetric, and the order of  $i$  and  $j$  is irrelevant (e.g.  ${}^2 L_{Ga,In} = {}^2 L_{In,Ga}$ ). For the  $v = 1$  term however, the expression is antisymmetric and the ordering of  $i$  and  $j$  is important ( ${}^1 L_{Ga,In} = -{}^1 L_{In,Ga}$ ).

While a lot of binary systems have reported interaction parameters for many phases, the ternary counterparts are less prevalent. For an As-Au-Ga mixture, the ternary excess energy covers the change in energy due to specific combination of materials which is not covered by a linear combination of the binary systems. The excess ternary mixing energy is commonly expressed as  $E g_{i,j,k} = X_i X_j X_k L_{i,k,j}$ . The interaction parameter  $L_{i,k,j}$  is often reported as a constant, is sometimes given as temperature dependent, but can ideally be found as a function of  $X_i, X_j, X_k$  to describe asymmetric effects.

In some situations, a ternary system is easier to treat as a pseudobinary, for instance when it comes to ternary III-V semiconductors like InGaAs<sup>40</sup>. The In and Ga are randomly distributed in the group III sites of the lattice, but the As occupies all group V lattice

sites. This means that the excess energy of the  $InAs_{1-x}GaAs_x$  system can be described using Equation 8.

Probably the most well known use of thermodynamics for materials science is in the construction of phase diagrams. When the thermodynamics for a particular materials system is being assessed, the goal is typically to find values for the parameters in Equations 6-8. If these values are known, it is possible to calculate the energy for each phase for the system at each temperature and composition. From there, it is straight forward to find the phase or phases which minimize the energy of the system at any given temperature and composition, and from there generate equilibrium phase fields for the entire parameter space.

However, thermodynamics has uses beyond finding the equilibrium of a system; this framework can also be used to evaluate the driving force for phase transformation. Commonly, this is done using chemical potentials,  $\mu_i^p$ , instead of the total energy. The chemical potential is defined as:

$$\mu_i^p \equiv \left( \frac{\partial G^p}{\partial n_i} \right)_{T,P,n_{j \neq i}} \quad (9)$$

With the provided framework for  $g^p$  this derivation is, although tedious, possible to do.  $G^p$  is the total energy of the system which is found by multiplying  $g^p$  with the total size of the system,  $g^p \sum_j n_j$ , and all molar fractions can be rewritten as  $X_i = n_i / \sum_j n_j$ . After finding the relevant chemical potentials for one phase, the process is repeated for another phase, and then we can evaluate the supersaturation for a particular phase transformation,  $\Delta\mu$ . For the solidification of liquid Ga and As into Zinc Blende GaAs, I define the supersaturation as:

$$\Delta\mu = \mu_{Ga}^l + \mu_{As}^l - \mu_{GaAs}^{ZB} \quad (10)$$

If this supersaturation is positive, then the energy of the system would be reduced by forming solid GaAs. The value of the supersaturation describes how energetically favorable the solidification is, which is important when it comes to the kinetics of the solidification. The kinetics, and the influence that the supersaturation has on the solidification, will be covered much more in detail in Section 4.

### 3.1 Zinc Blende & Wurtzite

The content of this thesis focuses on the VLS growth of III-V nanowires, meaning that the solid phases of interest are those that can be formed by III-V materials. In the nanowire

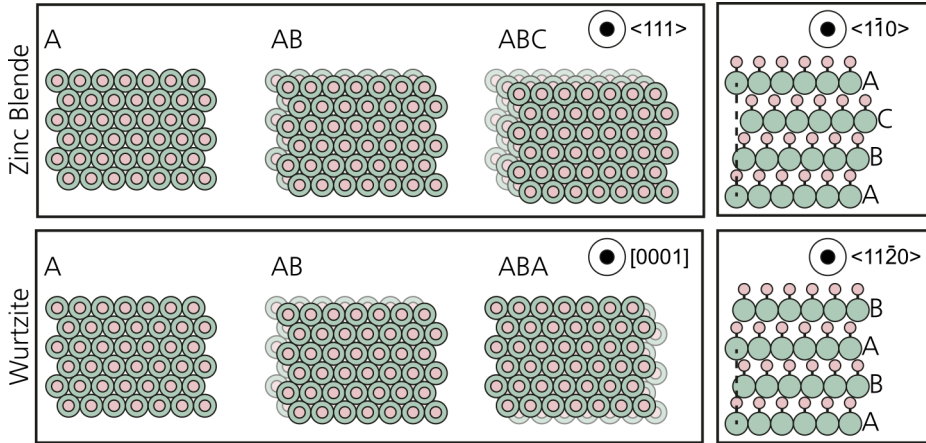


Figure 8: The atomic arrangement for the ZB and WZ structures.

form, most III-V materials can solidify in two specific crystal structures; the Zinc Blende (ZB) and the Wurtzite (WZ) structure. For nitrides, WZ is the stable structure, i.e. the one with the lower chemical potential. For all other III-V materials, ZB is the stable of the two.

Viewed from specific crystallographic directions ( $\langle 111 \rangle$  in ZB and  $[0001]$  in Wurtzite), the two structure are very similar as is shown on the left hand side in Figure 8. From this perspective, both structures consist of hexagonally close packed planes of III-V pairs. The difference is in how these hexagonally close packed planes align with their neighboring planes. For ZB, three sequential layers form a repeating unit (...ABCABCABC...), which is seen from a side view on the right hand side in Figure 8. For WZ, the repeating segment instead consists of two layers (...ABABAB...).

This slightly changes the local environment for each atom in the lattice and in WZ, the III-V pairs are a bit closer to its next nearest neighboring pair compared to the ZB structure. The shift in energy is rather slight, with estimated values ranging from around -45 meV per III-V pair for AlN<sup>41</sup> to around 25 for GaSb<sup>42</sup>. This difference in bulk cohesive energy between the two phases are labelled  $\psi$ , and is the reason why for instance WZ GaAs is not seen in bulk form.

In addition to having different bulk cohesive energies, the two structures also have different surfaces, which can be seen in the right hand side of Figure 8. Specifically, for nanowires growing in the  $\langle \bar{1} \bar{1} \bar{1} \rangle / [000\bar{1}]$  directions, the surfaces which commonly form the vertical sidewalls of the nanowires are different for the two structures<sup>43,44</sup>. While there is a wide spread in the estimates found in literature of what the actual energies of these surfaces are, most of the reports agree that the WZ  $\{10\bar{1}0\}$  surface should have a lower surface energy than the ZB  $\{1\bar{1}0\}$  surface<sup>43,44,45,46,47</sup>.

### 3.2 Miscibility Gap

In many binary and pseudo-binary systems, where the two pure components exhibit the same structure, it is favorable for the two components to intermix, and the position of each atom or component is completely random. This is due to the entropy of mixing (second sum in Equation 7), which always reduces the energy of a random mixture. However, there are some systems where this mixing is unfavorable. For solids, this is typically due to differences in the size of the two components. For very large differences, the two components are typically completely immiscible over the entire composition and temperature range. However, when the size difference between the components are 'reasonably small', the system can have a miscibility gap. This results in the components being miscible for some combinations of temperature and composition, and immiscible for other combinations.

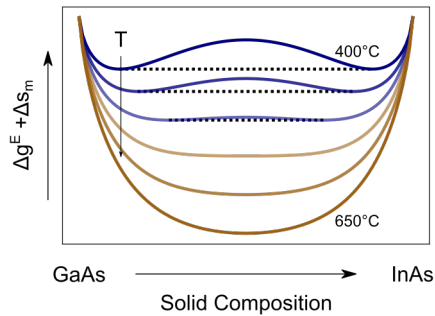


Figure 9: The entropy of mixing plus the excess Gibbs free energy of mixing, plotted for temperatures between 450°C and 650°C, with intervals of 50°C. The dashed lines indicate the immiscible regimes.

One such system is the InGaAs system, where the solid ZB phase contains a miscibility gap. In this system the entropy of mixing (second term in Eq.7) is counteracted by the excess energy of mixing which for this particular system is expressed as  $g^E = x(1-x)L_{InAs,GaAs}(T)$ , where the interaction parameter  $L_{InAs,GaAs}(T)$  is positive for most temperatures. In Figure 9, the sum of both the entropy of mixing and the excess free energy is plotted for temperatures between 450°C and 650°C. Here it can be seen that the curve changes from having two local minima below 550°C to having a single minimum above 550°C. This means that from a purely thermodynamic perspective it should be impossible to form  $In_{1-x}Ga_xAs$  at compositions around  $x = 0.5$  at temperatures below  $\sim 550^\circ\text{C}$ .



## 4 Kinetics

Kinetics discusses the rates at which atoms can move, react, attach or detach. In crystal growth, this is often discussed together with thermodynamics; thermodynamics will tell you which phase has the lowest energy, and kinetics will tell you if that phase will form immediately, soon or in a billion years. While kinetics affects several aspects of the nanowire growth process; here, I focus on the nucleation process from a classical perspective following Ref 48.

### 4.1 Becker-Döring equations

The classical approach to the solidification process typically starts with the Becker-Döring rate equations. This builds on the idea that the solid forms and grows through the attachment and detachment of single monomers (a monomer can refer to e.g. a GaAs pair or a Si atom). This type of cluster growth is shown in Figure 10.

With this description we can construct a set of equations to describe how these clusters grow and shrink over time.

$$\frac{dc_i}{dt} = J_{i-1} - J_i = (\omega_{i-1}^+ c_{i-1} - \omega_i^- c_i) - (\omega_i^+ c_i - \omega_{i+1}^- c_{i+1}), \quad i \geq 2 \quad (\text{II})$$

Here,  $c_i$  is the concentration of clusters of size  $i$ , and  $J_i$  is the net rate at which a monomer and an  $i$ -sized cluster merge to form a  $i + 1$  sized cluster. These net rates can be expressed using the rate constants  $\omega_i^+$  and  $\omega_i^-$ , where  $\omega_i^+$  is a function  $c_1$ . Equation II only applies to clusters containing 2 monomers or more. For the smallest clusters, we instead have:

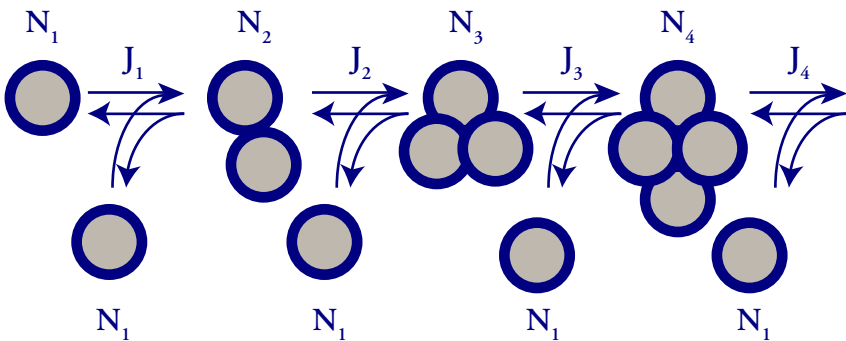


Figure 10: Schematic of the cluster growth process in the Becker-Döring equations.  $N_i$  represents a cluster of size  $i$ , and  $J_i$  is the net rate at which clusters of size  $i$  combine with a monomer to form a cluster of size  $i + 1$ .



$$\frac{dc_1}{dt} = -2J_1 - \sum_{i=2}^N J_i + N\omega_N^+ c_N \quad (12)$$

We imagine that clusters which grow beyond a very large size, labelled as  $N$ , are removed from the system, and replaced with an equal number of monomers. This gives a steady state, where the concentrations remain constant with a net growth of the system,  $J_i = J_{i+1} = J_0$ . This gives rise to:

$$\begin{aligned} J_0 &= \omega_1^+ c_1 - \omega_2^- c_2 \\ J_0 &= \omega_2^+ c_2 - \omega_3^- c_3 \\ &\vdots \\ J_0 &= \omega_{N-1}^+ c_{N-1} - \omega_N^- c_N \\ J_0 &= \omega_N^+ c_N \end{aligned} \quad (13)$$

Since clusters of size  $N + 1$  are removed from the system, the  $\omega_{N+1}^- c_{N+1}$  is not included in the last equation. Next, we multiply each of these equations by a ratio of rate constants, the first with  $1/\omega_1^+$ , the next with  $\omega_2^-/(\omega_1^+ \omega_2^+)$ , then  $\omega_2^- \omega_3^-/(\omega_1^+ \omega_2^+ \omega_3^+)$  and so on. If we start from the first equation, this treatment gives us:

$$\frac{J_0}{\omega_1^+} = c_1 - \frac{\omega_2^-}{\omega_1^+} c_2 \Leftrightarrow c_1 = \frac{J_0}{\omega_1^+} + \frac{\omega_2^-}{\omega_1^+} c_2 \quad (14)$$

By repeating for the second equation, we see that:

$$\frac{\omega_2^-}{\omega_1^+} c_2 = \frac{J_0 \omega_2^-}{\omega_1^+ \omega_2^+} + \frac{\omega_2^- \omega_3^-}{\omega_1^+ \omega_2^+} c_3 \Leftrightarrow c_1 = \frac{J_0}{\omega_1^+} + \frac{J_0 \omega_2^-}{\omega_1^+ \omega_2^+} + \frac{\omega_2^- \omega_3^-}{\omega_1^+ \omega_2^+} c_3 \quad (15)$$

Continuing this iteratively until the final cluster size,  $N$ , is reached gives:

$$c_1 = J_0 \sum_{i=1}^N \frac{1}{\omega_i^+} \frac{\omega_2^- \omega_3^-}{\omega_1^+ \omega_2^+} \dots \frac{\omega_i^-}{\omega_{i-1}^+} \Leftrightarrow J_0 = c_1 \left[ \sum_{i=1}^N \frac{1}{\omega_i^+} \frac{\omega_2^- \omega_3^-}{\omega_1^+ \omega_2^+} \dots \frac{\omega_i^-}{\omega_{i-1}^+} \right]^{-1} \quad (16)$$

This equation is the foundation for the steady state nucleation rate within the Becker-Döring framework. The most common way to move forward with this equation, ends with the classical nucleation theory, which will be covered next.

## 4.2 Classical Nucleation Theory

A cluster is difficult to assess from an energy perspective. As discussed in the thermodynamic section, the energy of an atom is sensitive to many factors; the local temperature, the composition of the mixture and, if it is in a solid phase, how the atoms are arranged. In the thermodynamic framework, the energy of the system is based on the idea that the system can be treated as infinite, but clusters of the sizes discussed here are far from infinite. If you have a cluster of 13 atoms, arranged in the face centered cubic structure, only one of those atoms will have a complete set of nearest neighbors, and no next-nearest neighbors. None of them will have the same energy as an atom in the corresponding infinite bulk.

To treat clusters from an energy perspective, the most common approximation is to split the energy contributions of the atoms into two parts, the bulk contribution and the surface contribution. In the bulk contribution, the energy of all the atoms are added, as if they are part of an infinitely large system. If the thermodynamic parameters are known for the particular materials system, this is the energy we can calculate using the framework described in Section 3. The difference in energy between the real cluster and this bulk cluster is condensed into the surface contribution. The cluster is imagined having an infinitely thin surface layer, which has a certain surface energy associated with it. In the commonly used capillary approximation<sup>49</sup>, this surface energy (per unit area) is assumed to be independent of the size of the system. Thus, if there is a thermodynamic database for a materials system, and the specific surface energy is known or estimated, then the energy of the cluster can be calculated.

Consider the change in free energy of forming a spherical liquid cluster from a surrounding vapor phase.

$$\Delta G(r) = -\frac{4\pi r^3}{3\Omega_L}\Delta\mu + 4\pi r^2\sigma \quad (17)$$

The two terms represent the bulk contribution and the surface contribution respectively and are a function of the radius of the cluster,  $r$ . The volume of a sphere is  $4\pi r^3/3$  and, divided by the atomic volume of a monomer ( $\Omega_L$ ), this results in the number of monomers in the sphere. Each monomer has lowered its energy by the supersaturation of the system  $\Delta\mu$ . On the other hand, a surface with the area of  $4\pi r^2$  has been created, which increases the free energy of the system via its surface energy (or surface tension, which is the common terminology for a liquid-vapor interface),  $\sigma$ .

The trend in the formation energy when changing the radius is shown in Figure 11. Because of the surface to volume ratio, the energy of very small clusters is dominated by surface effects, and the energy of very large clusters is dominated by the bulk energy. In kinetics, typically the point of interest is the maximum formation energy, which represents the largest

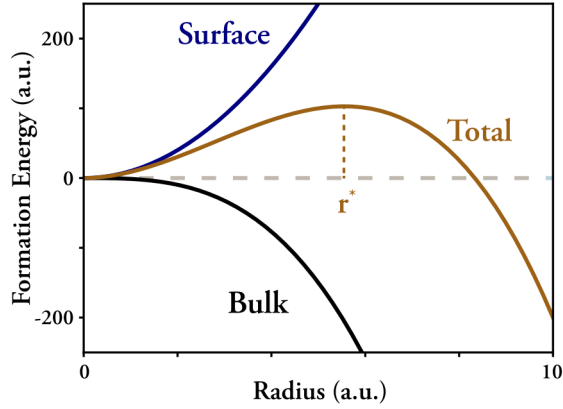


Figure 11: Visualization of the formation energy of a cluster. Due to the difference in radius dependence of the surface and bulk terms in Equation 17, the total energy reaches a maximum at the critical size. This radius is marked as  $r^*$  in the graph.

value in Equation 17, and is found at a critical radius  $r = r^*$ . For clusters which are larger than this critical size, it is energetically favorable to continue to grow. For smaller clusters, it is energetically favorable to shrink. To evaluate this energy barrier for nucleation, the derivative of Equation 17 is set to zero:

$$r^* = r \Big|_{\frac{d\Delta G}{dr}=0} = 2\sigma\Omega_L/\Delta\mu \quad (18)$$

Now, looking at  $\Delta G(r^*)$  gives the so-called nucleation barrier:

$$\Delta G(r^*) = \Delta G^* = \frac{16\pi\sigma^3\Omega_L^2}{3\Delta\mu^2} \quad (19)$$

This gives the general expression for the nucleation barrier for a sphere. The procedure can be repeated for any type of shape, and for a solid with different facets the generic surface tension can be replaced with a sum of different surfaces  $4\pi r^2\sigma = \sum A_k\gamma_k$ . However, the general trends remain the same. The nucleation barrier becomes larger for clusters with a large surface energy, and smaller when the supersaturation is large.

For reasons which will become clear later, it is also convenient here to rewrite Equation 17 in a different way. Instead of using the radius of the cluster as a descriptor for the size, one can substitute it with the number of monomers ( $i = 4\pi r^3/3\Omega_L$ ), and also use Equation 18 to instead express the supersaturation as the corresponding critical size. This yields:

$$\Delta G(i) = \sigma \left( \frac{4\pi\Omega_L^2 i^{*2}}{3} \right)^{1/3} \left( 3 \left( \frac{i}{i^*} \right)^{2/3} - 2 \frac{i}{i^*} \right) \quad (20)$$

With Equation 20 in mind, we return to the Becker-Döring nucleation rate and explain how this can be approximated into the Classical Nucleation Rate. First, the attachment/detachment rates can be expressed if we approximate the cluster distribution to be in equilibrium, meaning  $J_0 = 0$ . This gives:

$$\omega_{i-1}^+ c_{i-1} = \omega_i^- c_i \Leftrightarrow \frac{c_i}{c_{i-1}} = \frac{\omega_{i-1}^+}{\omega_i^-} = \left( \frac{\omega_i^-}{\omega_{i-1}^+} \right)^{-1} \quad (21)$$

Now, we need to find a suitable expression for the rate constants. For clusters surrounded by vapor, this can be expressed as the ratio between the monomer partial pressure ( $P_v$ ) and the vapour pressure of the cluster,  $P_i$ :

$$\frac{\omega_i^-}{\omega_{i-1}^+} = \frac{P_i}{P_v} \quad (22)$$

The vapor pressure of the cluster can be calculated using the Kelvin equation:

$$kT \ln \frac{P_i}{P_\infty} = \frac{2\sigma\Omega_L}{r_i} \quad (23)$$

This can also be done for the monomer partial pressure. The partial pressure could be expressed as an overpressure, or alternatively as a supersaturation. Here, it is instead expressed as the critical radius of a cluster with which it is in equilibrium using Equation 18:

$$kT \ln \frac{P_v}{P_\infty} = \Delta\mu = \frac{2\sigma\Omega_L}{r^*} \quad (24)$$

This leads to a ratio:

$$\frac{\omega_i^-}{\omega_{i-1}^+} = \frac{P_i}{P_v} = \exp \left( \frac{2\sigma\Omega_L}{kT} \left( \frac{1}{r_i} - \frac{1}{r^*} \right) \right) = \exp \left( \frac{2\sigma}{kT} \left( \frac{4\pi\Omega_L^2}{3} \right)^{1/3} \left( \frac{1}{i^{1/3}} - \frac{1}{i^{*1/3}} \right) \right) \quad (25)$$

Now, Equation 21 can be extrapolated down to the concentration of monomers using Equation 25:

$$\frac{c_1}{c_i} = \prod_{k=2}^i \frac{\omega_k^-}{\omega_{k-1}^+} = \exp \left( \frac{2\sigma}{kT} \left( \frac{4\pi\Omega_L^2}{3} \right)^{1/3} \sum_{k=2}^i \left( \frac{1}{k^{1/3}} - \frac{1}{i^{*1/3}} \right) \right) \quad (26)$$

The sum can be replaced with an integral and solved. Under the assumption that  $i^* \gg 2$ , this yields:

$$\prod_{k=2}^i \frac{\omega_k^-}{\omega_{k-1}^+} \approx \exp \left( \frac{\sigma}{kT} \left( \frac{4\pi\Omega_L^2 i^{*2}}{3} \right)^{1/3} \left( 3 \left( \frac{i}{i^*} \right)^{2/3} - 2 \frac{i}{i^*} \right) \right) \quad (27)$$

By comparing this result to Equation 20, we see that the exponent is the same as the formation energy of the system:

$$\frac{c_i}{c_1} = \left( \prod_{k=2}^i \frac{\omega_k^-}{\omega_{k-1}^+} \right)^{-1} = \exp \left( \frac{-\Delta G(i)}{kT} \right) \quad (28)$$

Returning now to the Becker-Döring nucleation rate, and using Equation 28 to rewrite the ratio of rates using the formation energy, we are left with:

$$J_0 = c_1 \left[ \sum_{i=1}^N \frac{1}{\omega_i^+} \frac{\omega_2^-}{\omega_1^+} \frac{\omega_3^-}{\omega_2^+} \cdots \frac{\omega_i^-}{\omega_{i-1}^+} \right]^{-1} = c_1 \left[ \sum_{i=1}^N \frac{1}{\omega_i^+} \exp \left( \frac{\Delta G(i)}{kT} \right) \right]^{-1} \quad (29)$$

The last step before landing on the classical nucleation rate, is to resolve the sum. This is done using a few approximations. First, the remaining attachment rate is approximated to be independent on  $i$  in the region of interest, which is near the critical size of the cluster. This is reasonable for clusters where the critical size is large, since a cluster of 1000 monomers and a cluster of 1001 monomers have roughly the same surface area, and thus roughly the same attachment rate. Next, instead of using  $\Delta G(i)$  to express the formation energy, its Taylor expansion around the critical size (up to the second order) is used instead:

$$\Delta G(r) \approx \Delta G^* - \Delta G^*/3i^{*2}(r - r^*)^2 \quad (30)$$

The accuracy of this approximation again depends on critical size of the nucleus, which is shown in Figure 12. For large critical sizes, which is equivalent to a low supersaturation (see

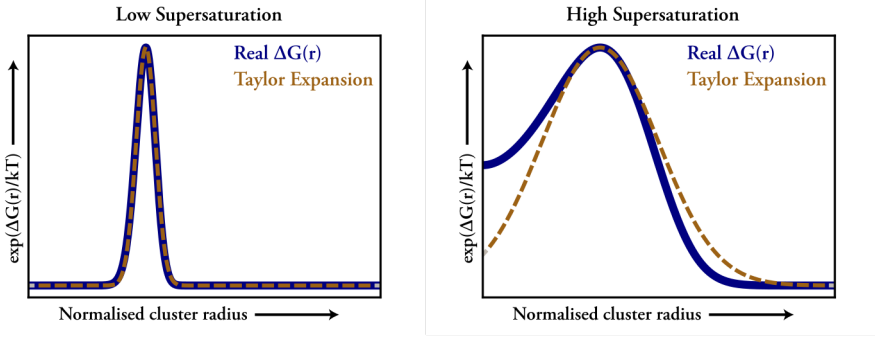


Figure 12: Graphs showing the accuracy of the Taylor expansion for the nucleus energy at low (a) and high (b) supersaturation.

Equation 18), this approximation is excellent. However, when the supersaturation becomes high, and the critical size smaller, this approximation becomes significantly worse, which is important to keep in mind.

In the expanded form,  $\exp((\Delta G^* - \Delta G^*/3t^{*2}(r-r^*)^2)/kT)$  leaves a constant  $\exp(\Delta G^*/kT)$ , and the Gaussian function  $\exp(-\Delta G^*/3t^{*2}(r-r^*)^2/kT)$ . Here, the finite sum over the Gaussian function is approximated by an integral from minus to plus infinity, since the infinite integral has a solution. This is motivated by the idea that  $\exp(\Delta G(r))$  rapidly reaches zero away from the critical size (as shown in Figure 12). Performing the integration finally results in:

$$J_0 = \omega_*^+ Z c_1 \exp\left(-\frac{\Delta G^*}{kT}\right) \quad (31)$$

This is the nucleation rate in the Classical Nucleation Theory. The Gaussian integral results in the so called Zeldovich Factor (which here becomes  $Z = \sqrt{\Delta G^*/3\pi kTt^{*2}}$ ), the attachment rate of a monomer onto a cluster of the critical size,  $\omega_*^+$ , the concentration of monomers,  $c_1$  and the exponential dependence on the nucleation barrier  $\exp(-\Delta G^*/kT)$ . While the derivation here was done for a sphere in vapor, the final expression can be tailored to other shapes and sources.

Equipped with an understanding on the origin and approximations of the nucleation rate of the classical nucleation theory, it is now time to turn and discuss how this has been used by me and other researchers in the field of nanowire growth.



# Modeling Nanowire Growth

In this part, the focus will shift to the work I have performed and contributed to during my studies. Throughout my studies, the goal has been to expand on the fundamental understanding of the nanowire growth, and while I have partaken in the experimental growth of nanowires, my main contributions have been through creating and using theoretical Monte Carlo simulation frameworks. The background knowledge found in the previous part was meant to aid the reader in following the Papers included in the thesis. Therein all the details regarding all the work which has been done can be found. In this part, I will cover my contributions, but I will attempt to focus more on that which is not in the papers, and that which transcends the papers. Therefore, a reading of the Papers in question is advised at this stage.

Nanowire growth is difficult to assess for the reasons discussed in Section 1: One can control the vapor phase composition of the precursor molecules and observe the solid nanowire after growth, but the actual growth of the wires happens via the intermediary liquid seed particles. Until very recently, it has been impossible to directly observe and study the seed particles during growth. Thus, much of the theoretical modeling for nanowire growth has been focused on a subset of the entire process, e.g. examining only the second transition from the liquid seed to the solid wire. In this way, aspects such as crystal structure selection<sup>36,50</sup> and ternary nanowire composition<sup>51,52</sup> have been modeled. These analytical models typically result in a phase field where a certain outcome is estimated (e.g. the probability of forming ZB, or which ternary composition has the lowest nucleation barrier) given a certain liquid state. Because these models operate on a subset of the entire process, interpretations of the results require assumptions to connect to experimental results where the state of the intermediate liquid is unknown, e.g. that a higher arsenic flow in the vapor means a high supersaturation in the liquid.<sup>15</sup> Alternatively, there are many models focusing on the other subset, the vapor (or adatom) to liquid transition. This approach has mainly been used for studying mass transport limited growth<sup>53</sup>.

There have been works which combine both the vapor-liquid transition and the liquid-solid transition into one single analytical model<sup>54,55,56,57</sup>, which typically involves the assump-



tion of stationary growth, which includes a constant composition in the liquid. Steady state nanowire growth, where the vapor phase composition is maintained throughout long periods of growth is however cyclical<sup>58,59</sup>. There are periods of incubation, where the seed particle incorporates more and more growth species and become increasingly supersaturated with respect to the solid phase. These incubation periods end with a nucleation, where the nucleation barrier is surpassed and a stable nucleus is formed. Because of the nanoscale size of the seed particle, this will deplete the droplet of some of the accumulated growth species and cause the composition to change.<sup>60</sup> After nucleation and depletion, the stable nucleus grows slowly as the limiting species arrive via impingement or diffusion until a complete layer has formed. This means that even if one knew the exact averaged composition over several cycles, using this value will always underestimate the supersaturation at the moments of nucleation and always overestimate the supersaturation during the propagation of the stable nucleus into a complete layer.

While the analytical approaches tend to have these drawbacks, the tremendous amount of work that has been put into these models have greatly advanced the fundamental understanding of nanowire growth. However, it remains difficult to compare the theoretical results to experimental results. As an example, during experimental growth one is free to tune the precursor flows in the vapor, but it is not clear how that in turn can tune the supersaturation in the seed particle or the nucleation barrier. The results of static analytical models are also difficult to reconcile with the dynamic nature of nanowire growth. My work with creating Monte Carlo simulation frameworks was mainly performed for these reasons. I aimed to bridge the theoretical insights with the experimentally accessible parameters, minimizing the need to make additional assumptions in order to extrapolate the theoretical results to experimental growth, while also capturing the impact that the dynamic nature has on the growth. In the following section, I will outline how such simulation frameworks can be constructed.

## 5 Simulation Frameworks

In this section I will bring up the building blocks and modeling decisions relevant for my simulation frameworks, and discuss how the available choices may affect the final model. This is intended to be a guide for anyone interested in creating a simulation model for themselves.

### 5.1 Time

The frameworks I have worked with can be separated into two categories based on how they handle time. In one category, the simulation progresses in pre-determined time-steps. This static step approach was used in Papers II,III and IV. The second category instead utilized a continuous time-line, and this approach was used in Paper V.

In the continuous time-line, time progresses via individual events such as the impingement of a single Ga atom, the evaporation of a single As atom, or the solidification of a single GaAs pair. The time it takes between the previous event and the next depends on the individual rates of all events at that moment and, as discussed in the example with photon scattering in Section 2, a time-step can be generated using Equation 5. While this approach has several benefits, which will be discussed in the different subsections below, it has one significant downside: Computationally, it is time consuming. As a reference; the simulations performed in Paper V took roughly one hour real time for each second of simulated time. This computational time also scales very unfavorably with the size of the system, which effectively makes lengthy growth recipes and large nanowires unfeasible to study.

Instead of individual events one at the time, one can instead look at averages over a set time step, as is done in the static step frameworks. This results in a much more efficient framework in terms of computational time and does not suffer from the same poor scaling with size. This is perhaps best highlighted in Paper III, where I simulated long growths with varying nanowire radii. A back of the envelope calculation indicates that one simulation with the largest particle used in Paper III would take approximately 8 months to perform using the continuous time model of Paper V. The downside of the static step approach is that it limits the models to only look at averages over that time period: Instead of impingement and evaporation of individual atoms, one is limited to net condensation. Instead of attachment and detachment of III-V pairs to an unstable nuclei, one is limited to look at nucleation as a singular event. These differences will be discussed more in their respective subsection.

It should be noted that in terms of accuracy, the models utilizing a continuous time-line should be able to capture more nuances in the growth. Thus, this is the approach which I would generally recommend one to use, should the computational time allow for it.

## 5.2 Vapor-Liquid

Here, I address how the transfer of material from the vapor phase to the liquid phase has been treated in my works. For VLS growth, the growth species can arrive to the liquid seed particle using different pathways; either directly from the vapor phase through direct impingement or via the adatom phase through the diffusion process. There is consensus that impingement is the most common pathway for many group V species<sup>61,62</sup>, whereas many group III species tend to take the surface diffusion pathway<sup>53,62,63</sup>.

For impingement, I have used the well known and widely used (Hertz-)Knudsen equation<sup>53,64,65</sup> to calculate the impingement rate in all of my models:

$$J_{Imp,i} = A_{LV} \frac{\alpha P_i}{\sqrt{2\pi m_i k_B T}} \quad (32)$$

This gives the impingement rate for species  $i$  in units of atoms per second, which depends on the area of the liquid-vapor interface  $A_{LV}$ , the pressure of the species in the vapor phase,  $P_i$ , and the atomic mass of the species,  $m_i$ .  $\alpha$  is a sticking coefficient which can be used if a particular species is unlikely to attach to the surface upon impingement. In the models this has been set to 1, and is thus ignored, due to the treatment of the supply pressure  $P_i$ . In the simulations I have performed, the input values for  $P_i$  are not intended to be directly comparable to experimental pressures. In MOVPE growth, the growth species are supplied in their precursor form and must decompose before depositing the atomic species to the seed particle. Due to the complexity of the decomposition process<sup>24</sup>, I did not attempt to incorporate this aspect into the frameworks. This means that when looking at the results of Papers II-V, it is important to keep in mind that only the trends are important and not specific values for the pressure in the vapor.

For evaporation, I have used the corresponding Hertz-Knudsen equation:

$$J_{Ev,i} = A_{LV} \frac{\eta P_{eq,i}}{\sqrt{2\pi m_i k_B T}} \quad (33)$$

The difference here is that the sticking coefficient  $\alpha$  has been replaced with a corresponding evaporation efficiency,  $\eta$ , and the pressure is now the equilibrium pressure  $P_{eq,i}$  and not the supplied pressure. One could also consider the evaporation of molecules instead of atoms, which would add an additional pre-factor<sup>66</sup>. The equilibrium pressure varies greatly for different species, and variables like the temperature and the composition of a mixture. It is difficult to find reasonable values for the equilibrium pressure at growth conditions, and I have used different approaches for estimating the actual pressure. This varies from using fixed, temperature independent values for Paper II, to incorporating temperature- and

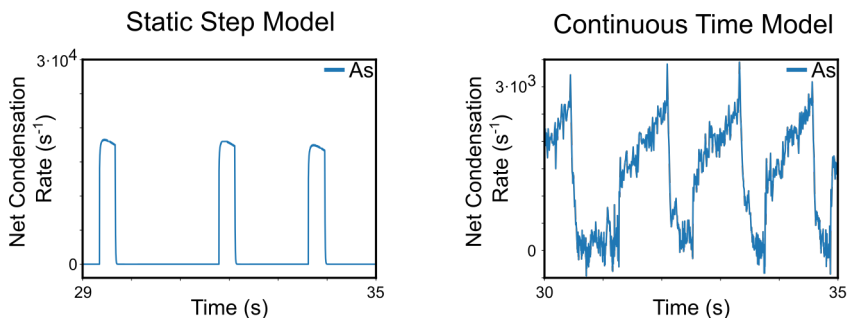


Figure 13: Graphs comparing momentary net condensation rates for As using a static step model and a continuous time model.

composition-dependencies in Paper v. To the best of my knowledge, the expression for the evaporation efficiency is unknown which has led me to use  $\eta$  as a pure fitting parameter.

For simulations performed in the static step frameworks, the actual rate used is the difference between the impingement and evaporation rates since each time step typically covers hundreds or thousands of individual events. In the continuous time framework, impingement and evaporation are treated as separate events which causes some noticeable differences compared to the static step framework, as is shown in Figure 13 for the As species. Here it can be seen that the net condensation rate for the static step approach is very smooth, and in the incubation periods it rapidly goes to zero. This of course translates to a very smooth and stable molar fraction of As. The continuous time approach on the other hand shows significant fluctuations in the net condensation rate, corresponding to a fluctuating molar fraction of As. Since it captures this aspect of the growth process, the continuous time model may thus be suitable for studying the effect that the fluctuations may have on the nucleation step.

While condensation has been the main pathway I have used for my simulations, I also considered diffusion in Paper III. When studying the effect of varying the nanowire radius, it is important to use diffusion as the pathway since it is known to have a great effect on the radius-dependent growth rate<sup>53,67</sup>. Typically, the rate limiting step can be thought of as either diffusion along the sidewall of the nanowire or substrate diffusion. These choices represent different geometries which, together with the choice of boundary conditions and material parameters, lead to different dependencies (an interested reader is referred to Chapter 4.8 in Ref 68). However, for the simulations performed in Paper III, and the trends found in the results therein, the important part is that all diffusion pathways scale differently with nanowire radius compared to impingement. Thus, the details in the expression for the diffusion rate are of great importance when matching analytical expressions for Length-Radius dependencies with experimental results, but not for the fundamental understanding of the dynamics in the seed particle which I focused on in Paper III.

### 5.3 Liquid-Solid

Next, I address the growth of the solid nanowire from the liquid seed, starting with the nucleation step. The word nucleation is sometimes used to describe the very first stage of experimental nanowire growth<sup>69</sup>. This is the stage where the initial seed particles start to alloy with the substrate and/or supplied growth species, leading to a supersaturated seed particle and finally the growth of the first layer of the nanowire. The reason for distinguishing this stage of growth is that it may require special care with different growth parameters or even materials than the following continuous growth<sup>70</sup>. However, for the purpose of this thesis I refer to nucleation as the process wherein monomers from the supersaturated liquid phase form a nuclei at the seed particle-nanowire interface which, after growing beyond its critical size, becomes stable. The term nucleus can refer to both unstable/sub-critical and stable/super-critical clusters.

In Section 4 I presented the classical nucleation theory(CNT), and the descriptions therein forms the basis for how I have approached nucleation in my work. For Papers II-IV, I worked with an adaptation of the full expression for the classical nucleation rate in Equation 31, whereas for Paper V I used the attachment and detachment of individual III-V pairs to treat the liquid-solid transition. This stems from Figure 10, which is the starting point of the Becker-Döring equations.

A nucleus on a nanowire-seed particle interface represents a different geometry than the generic case discussed in Section 4, and this needs to be addressed. Firstly, as nanowires commonly grow layer by layer, the nucleus will be two- and not three-dimensional. This changes the supersaturation-dependencies of the nucleation barrier to  $\Delta G^* \propto \Delta\mu^{-1}$  as opposed to  $\propto \Delta\mu^{-2}$  for the 3D case.

The geometry of the nanowire-seed particle system and the shape of the nucleus, shown in Figure 14, will also affect the interface energies during nucleation. These factors will, as well as the supersaturation-dependence mentioned previously, enter the exponent of the nucleation rate. This means that the nucleation rate is very sensitive to the interface geometry and energies.

In literature, there have been many different descriptions of the shapes throughout the years. The nucleus shape has been treated as a semi-circle<sup>71</sup>, a triangle<sup>44,63</sup>, a hexagon<sup>72</sup>, or a rhombus<sup>73</sup>. There are also significant differences in the values for the surface energies in literature; the surface energy for the  $\{110\}$  facets of GaAs has reported values between 1.5 J/m<sup>2</sup> using dangling bonds calculations<sup>44</sup> to around 0.6 J/m<sup>2</sup> using ab-initio methods<sup>45</sup>. In addition, there is consensus in the research field that nucleation mainly occurs at the triple phase line (TPL)<sup>36</sup>, i.e. around the perimeter of the nanowire-seed particle interface. This has the implication that a part of the sidewall of the nucleus becomes surrounded by the vapor phase, whereas the rest of the perimeter is surrounded by the liquid phase

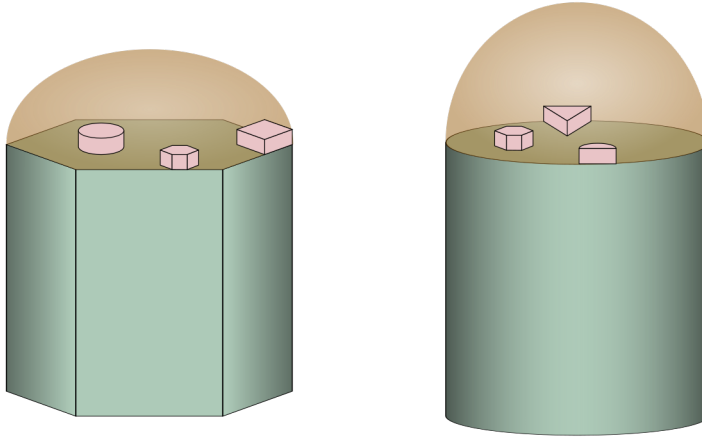


Figure 14: Schematic of several possible nanowire and nuclei geometries.

of the seed particle. This choice position affects the energetics of the nucleus, since the vapor-solid interface energy ( $\gamma_{SV}$ ) is expected to be different than the liquid-solid interface energy ( $\gamma_{SL}$ )<sup>74</sup>. Positioning the nucleus at the TPL also has the effect that part of the sidewall of the nucleus replaces part of the vapor-liquid surface area, which will reduce the energy of the liquid-vapor interface. Thus, replacing part of the low-energy SL-interface with the higher-energy LV-interface leads to a reduction in the total interface energy of the nucleation due to the removal of part of the LV-interface.

These modeling choices, of how to describe the nucleation and which energies to use, matter because they (all else being equal) have a large effect on the size of the nucleation barrier. The crystal structure selection (which is discussed further in Section 6) depends on the relative nucleation rate of WZ and ZB, and then these modeling choices will matter. The choices will affect the momentary nucleation rate which will affect the steady state composition of the seed particle, and the dynamics of a growth cycle (as is discussed further in Section 7). For ternary nanowires, these choices will also have an effect on the relative growth rate of the two binary III-V materials (which is discussed further in Section 8).

It is important to keep in mind that the details and values surrounding these modeling choices are approximated for specific conditions at best, and generally unknown or speculation at worst. However, trends in these details are generally more reliable. As an example, I do not know whether the surface energy of the GaAs  $\{110\}$  facets is closer to  $1.5 \text{ J/m}^2$  or  $0.6 \text{ J/m}^2$  during typical nanowire growth conditions, but it is reasonable to assume that it is higher than its WZ counterpart or its InAs counterpart (by comparing values from Refs 43,44,45,47,75,76)). Thus, the results from this type of modeling should be treated as such; the details are often as uncertain as the input values, but the emerging trends are typically

much more robust and thus, much more interesting to discuss.

From a temporal perspective, the static step models assume an instantaneous transition from no nucleus to a barely stable nucleus; whereas in the continuous model, the nucleus is constantly growing and shrinking in the sub-critical size regime until it becomes large enough to stabilize. It is not clear to me whether the static step models are by definition less accurate than the continuous time models when it comes to capturing the nucleation process. The depletion effect\* is often neglected in nucleation models, but can be incorporated both into analytical models<sup>60</sup> and in the simulations as in Paper IV. On the other hand, to some extent a sub-critical nucleus could act as a potential 'III-V buffer' for growth material during incubation, which would partially counteract the depletion effect. It is also uncertain whether nanowire growth occurs under high enough supersaturation to limit the accuracy of the Taylor expansion used in CNT, as discussed around Equation 30.

The clear benefit of the continuous time model is that many of these potential 'variations' or uncertainties of the nucleation process are by default incorporated into the simulations even if they are not specifically added in the code. Depletion and potential buffer-effects arise naturally from the dynamics, but it is unclear if these aspects can be accounted for if the entire nucleation process is condensed down into one step. I would also like to add here that the choice of framework also depends on whether the intended nanowires are binary or ternary. For ternary nanowires, it is unclear to me how to implement an accurate representation in the static step framework.

## 5.4 Step Flow

After nucleation, the now stable nucleus propagates across the L-S interface until a complete layer has formed. This step flow has been treated very differently in my models: In Papers II and III I was purely interested in the nucleation events and thus the step flow was neglected in these works. Practically, this meant that the propagation of the entire layer was assumed to be instantaneous, removing the corresponding amount of III-V pairs from the droplet. For Paper IV, I used the ideas of droplet depletion<sup>60</sup> to determine how far the layer will propagate until it is no longer thermodynamically favorable to do so. In each time step, the layer irreversibly and instantaneously grew to this point, until enough time had passed and enough growth species had impinged to fully complete the layer. In Paper V, the step flow is treated exactly the same way as the nucleation process; the (now super-critical) nucleus is free to grow and shrink at all times based on the momentary state of the system, progressing time whenever it changes. I consider both of these approaches to be reasonable for binary III-V growth.

---

\*if the seed particle is very small, removing III-V pairs from the liquid to form the critical nucleus can reduce the supersaturation in the liquid to the point where the previously stable nucleus becomes unstable

## 5.5 General Notes

It is worth commenting that it may seem like there are a whole lot of fitting parameters, and uncertainty in the values for the materials properties, in the simulation frameworks, and that this could make it difficult to trust that the parameters are reasonably chosen. By extension, this would imply that it is difficult to trust the results of the simulations. I find it very difficult to believe that each of the parameters I have used are 'correct compared to reality' in terms of their values. However, the full expressions are in most cases bounded by experimental observations. As an example, the growth rate of nanowires are typically on the order of nm/s for MOVPE growth, and since a GaAs nanowire consists of 50% As, this give a lower bound for the As flow such that  $J_{Imp,As} \geq dL/dt \times dN_{As}/dL$ . During GaAs growth, the flow of As is routinely increased and decreased by a factor of 100<sup>34</sup>, and if the evaporation is too low, this would lead to As accumulation and an unstable seed particle as a result. At the same time, the concentration of As in the seed particle is not quantifiable in composition measurements during nanowire growth inside a transmission electron microscope<sup>77</sup>, which indicates that  $X_{As}$  should be low at most, if not all, times. Criteria such as these serve to balance all of the different materials- and fitting parameters into reasonable ensembles.





## 6 Crystal Structure Selection

Here, I will go more in depth regarding the topic of crystal structure selection in nanowire growth. I give a very brief presentation of some well known experimental trends and theoretical understanding, and discuss how this connects to the results of Papers I-III.

### 6.1 Experimental Trends

Here, I will present an overview of general experimental trends of the crystal structure selection when it comes to the growth of nanowires, which connect to my research. While the trends are general in nature\*, I will focus on presented results from the GaAs materials system, as it is the main III-V material I have used in my research.

A common way to tailor the crystal structure of the nanowires in MOVPE growth is by controlling and changing the precursor flows. This is commonly done by changing the V/III ratio, mainly by increasing or decreasing the group V pressure<sup>11,78</sup>. Under normal MOVPE growth conditions, a high AsH<sub>3</sub> flow (high V/III ratio) leads to ZB GaAs nanowire whereas a low AsH<sub>3</sub> flow (low V/III ratio) results in nanowires with the WZ structure. For GaAs wires grown using molecular beam epitaxy (MBE), the opposite behavior is typically observed, where a high flux of As promotes the WZ structure and a low As flux leads to ZB growth<sup>15</sup>. This 'MBE-ZB regime' has also been observed in for MOVPE growth<sup>34</sup>, when the AsH<sub>3</sub> pressure is reduced beyond the normal growth conditions. It has also been shown that changing both the As and the Ga flows, keeping the same V/III ratio, has an effect on the crystal structure. A higher total flow resulted in a ZB nanowire with less stacking defects and WZ insertions, which is counter-intuitive as a high growth rate is typically associated with a higher defect density.<sup>79</sup> This clearly indicates that while there are methods for experimentally controlling the crystal structure in nanowires, the fundamental mechanism governing the selection is complex and non-monotonic.

There have also been reports that changing the initial seed particle material, in one way or the other, can affect the crystal structure. This can refer to either removing the Au and growing Ga-seeded nanowires<sup>80</sup>, introducing an additional dopant species to the seed before or during growth<sup>81</sup>, or exchanging some or all of the Au to another material<sup>20,82</sup>. In Paper I, the effect of exchanging all or part of the Au for Ag was studied in detail. Figure 15 shows images of nanowires grown using varying Ag:Au ratios under identical growth conditions, taken using transmission electron microscopy. These images show a clear increase in the WZ fraction of the wires grown with a Au:Ag ratio between 7:3 and 3:7 compared to the pure Au and Ag counterparts. This supplements the findings presented

---

\*at least for the (Ga,In)-(P,As) combinations

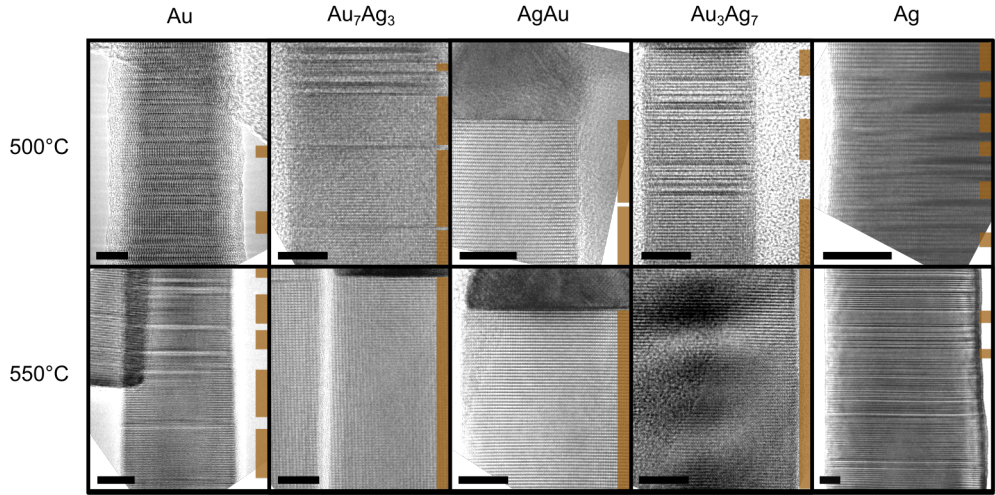


Figure 15: Transmission Electron Micrographs of GaAs nanowires seeded by various Ag:Au ratios. Nanowires from each row were grown in parallel under identical conditions (same as was used in Paper 1). Each row represents one growth temperature, each column represents one seed material. Scale bars represent 10 nm. The brown bars to the right in each panel are guides to the eye, indicating a distinguishable WZ segment longer than 5 ML. Images captured by Dr. R.R. Zamani.

in Paper 1, suggesting that alloying the Au particle with Ag does appear to promote the formation of WZ.

## 6.2 Theory

There have been many theoretical models for crystal structure selection in nanowires that have been created, modified, used and disused throughout the years. Herein I attempt to present some of the more undisputed knowledge regarding the topic.

First and foremost, WZ has a higher bulk cohesive energy than ZB for the III-V materials (excluding the nitride-family), which is what makes WZ metastable. The difference in cohesive energy  $\psi_{WZ}$  varies between different III-V materials. According to the topical review of Ref 41, the values range from  $23.1 \text{ meV/pair}$  for GaAs and  $24.6 \text{ meV/pair}$  for GaSb on the high end of the spectrum to  $10.6 \text{ meV/pair}$  for InP and  $8.0 \text{ meV/pair}$  for AlAs in the low end of the spectrum. This value will clearly have an effect on the crystal structure selection, as this dictates the difference in the supersaturation between the liquid phase and the two solid structures.

Another notable difference is that WZ is predicted to have a lower surface energy compared to ZB, as was mentioned in Section 3.1. Typically, in theoretical works where the sidewall surface energies for both structures are estimated, the WZ surface energy ranges between 65 % and 90% of the corresponding ZB surface<sup>43,44,45</sup>.

This combination, of WZ being metastable with a lower surface energy, means that WZ may be the lowest energy crystal structure for nanowires with a sufficiently small radius. This has been shown in several theoretical papers<sup>43,45,83,84</sup>, and the predicted transition radii for GaAs varies between a few nm to around 20 nm. However, WZ nanowires with much larger radii than the predicted transition radii are routinely grown, and 5 nm ZB wires have also been reported<sup>55</sup>. This leads to the consensus view that the crystal structure is determined by the nucleation event. Whichever structure that forms the stable nucleus will then grow into a complete layer, and it is very unlikely (under normal growth conditions) that this transform to another structure after the layer is completed, even if the grown structure is metastable.

Taking all this into consideration, a high supersaturation in the seed particle promotes the formation of WZ. The idea is that as the supersaturation (w.r.t. ZB) becomes higher, the difference in bulk cohesive energy  $\psi_{WZ}$  becomes more and more negligible. This is clear when considering the extreme cases: In the low end, if growth happens while  $\Delta\mu_{ZB} < \psi_{WZ}$  then WZ would not grow at all since the seed particle is not supersaturated with respect to solid WZ. The other end of the spectrum is illustrated by growth happening at 'infinitely' high ZB supersaturation, where  $\Delta\mu_{ZB} \gg \psi_{WZ}$ . This means that  $\Delta\mu_{WZ} \approx \Delta\mu_{ZB}$ , and the difference in supersaturation is negligible. Then, the lingering difference in surface energy results in WZ being promoted.\*

### 6.3 Simulations

My work has touched upon crystal structure selection in Papers I-III. Therein the full details regarding all the work can be found; here follows what I consider the combined key conclusions from these works, phrased in as general a way as possible.

The first point to highlight is that the experimentally controllable parameters determine the state of the seed particle during growth. These experimental parameters can refer to the commonly discussed parameters of precursor flows and temperature, but also to sample preparation steps such as seed material and particle positioning. In the simulations I have performed, the state of the particle has referred to the steady state composition of the seed particle, although this should extend to other factors as well. One such factor is the nanowire radius, but a dynamic nanowire radius has not been included in any of my simulation frameworks. In Paper I, we showed that the particle composition is correlated between different seed materials and AsH<sub>3</sub> flows via the chemical potential of Ga in the seed particles. This was made reasonable by the results of the simulations, wherein the As concentration was shown to rapidly reach a steady state situation where the evaporation rate equals the impingement rate. It is reasonable to assume that this holds for typical MOVPE

---

\*This is meant to illustrate the extremes cases. For a more complete picture of the high end, see Ref. 85

growth, since one can increase the flow of  $\text{AsH}_3$  by a factor 100<sup>34</sup> without causing continuous accumulation of As in the seed particles. The evaporation of As depends on the chemical potential of As in the seed, with a higher As fraction leading to a higher chemical potential and a higher evaporation rate. Thus, the system will find a steady state between the impingement and evaporation of As at some chemical potential (during the incubation periods where the system has enough time to find this steady state). This should result in fixed chemical potential of As across all particles for a given  $\text{AsH}_3$  flow, regardless of the initial seed material. The simulations in Paper II clearly show this correlation between the flow of As and the composition in the seed particle.

The next point is that nucleation will happen as fast as possible. This sounds obvious, but it does have some implications. As discussed previously, it is well known that the route to promote WZ is to increase the supersaturation in the liquid. From a thermodynamic perspective, this typically comes from increasing the molar fraction of either Ga or As in the seed particle<sup>86</sup>. However, as has been shown experimentally, increasing the flows of As and Ga does not necessarily result in the promotion of WZ<sup>79</sup>. Because nucleation happens as fast as possible, the simulations (mainly Paper II) show that the nucleation barrier remains roughly constant over a large parameter space. This means that in order to increase the supersaturation in the seed particle at the moments of nucleation, one should not consider how to increase the Ga and/or As fractions in the seed particle, meaning one should not try to forcefully increase the supersaturation. Instead, one should consider how to hinder nucleation as efficiently as possible. If the nucleus for instance has an extremely high surface energy of the sidewall facets, then a high supersaturation is required to get nucleation of any kind. If the supersaturation is high, then this helps the formation of WZ as discussed previously.

To nuance the previous point, the simulations of Paper III show that the cyclical dynamics of the nanowire growth cycle can also influence the crystal structure selection. In short, the more rapidly changing the system is (measured as how much the supersaturation varies with time), the higher the supersaturation will be when nucleation occurs. The simulations seem to suggest that this effect is not as impactful as the one previously discussed, however this could be dependent on the materials system and growth conditions. There are several ways to change the rate at which the supersaturation increases with time; a reduction in nanowire radius, an increase in the total flow, or a shift from a Ga-limited nucleation range to an As-limited nucleation range. All else equal, this should promote the formation of WZ. However, as is shown in Paper III, all else is rarely equal. Changing any one experimental parameter, whether it be the size of the initial seed particle or a precursor flow to achieve a higher growth rate, typically changes more than just the dynamics.

These results from the simulations are in line with the experimental hypothesis that exchanging some Au for Ag in the seed particle promotes the preferential nucleation of WZ. First, Ag has a significantly lower surface energy compared to Au<sup>87</sup>, and as a result, the

surface energy of the seed particle should be significantly lower with an increasing fraction of Ag (despite a slightly lower Ga fraction in the seed). During nucleation, a part of the liquid-vapor interface is effectively removed, and is replaced with the solid-vapor interface of the nucleus. This means that the lower the surface energy of the seed particle, the more difficult it is to nucleate GaAs from that seed. This should lead to nucleation at higher supersaturations for the Ag-rich particles.



## 7 Growth Dynamics

In this section, I attempt to cover the general topic of the dynamics of nanowire growth. Specifically, this refers to both dynamics relating to the incubation-nucleation-layer propagation cycle, as well as transient effects when the supply of growth species change. Some aspects of these dynamics can now be observed experimentally using in-situ methods, as was utilized in Paper iv, and for this reason I will also discuss the symbiotic nature of combining simulations and in-situ observations.

### Incubation, Nucleation & Layer Propagation

As mentioned previously, it is well known that the nanowires typically grow in cycles, one layer at the time. Each cycle is divided into a period of incubation, which ends with a nucleation event, and is followed by a period where the nucleus propagates across the liquid-solid interface until a complete layer has formed. This cyclic behavior is reflected in the particle composition, which oscillates roughly between an 'incubation composition' and a 'layer propagation composition', which is seen in the simulations of Papers iv and v. This can be understood, or generalized, by the knowledge that the seed particle is constantly striving towards an equilibrium with its surroundings. During incubation, there is a barrier for transferring material from the liquid to the solid phase, so the particle is moving towards an equilibrium with the vapor phase. During the step propagation, the barrier for solidification is gone, and the seed rapidly\* finds a liquid-solid equilibrium.

In Paper iv, I had the opportunity to collaborate with my co-authors who operate the in-situ environmental transmission electron microscope (eTEM) at the national Center for High Resolution Electron Microscopy in Lund<sup>89</sup>. In this eTEM, they were able to grow GaAs nanowires inside the microscope, using the regular MOVPE precursors TMG and AsH<sub>3</sub>, while having the observational powers of a TEM available during growth. Using the TEM, they collected measurements of the lengths of the incubation and layer propagation periods under varying AsH<sub>3</sub> flows in order to better understand the fundamentals of the dynamic growth cycle.

There are several advantages to combining these experimental measurements with simulations. Simulations can add value to the experiments since the simulations continuously generate all variables for the system (meaning the simulation is completely observable), and the only limit to the resolution of the simulation data is the user-chosen size of the static time step. This is important, for instance when it comes to the particle composi-

---

\*this can be seen in the simulations of Paper v, but there are other theoretical works to support the rapid equilibrium, see e.g. Ref. 88. This is also supported by the 'instantaneous' depletion of the seed particle after nucleation which is seen experimentally in Paper iv



tion. While it is possible to perform energy-dispersive X-ray spectroscopy (EDX) inside the  $\epsilon$ TEM during growth, EDX as a method has limitations in terms of its resolution. In my simulations, I typically find that the molar fraction of As is far below 1 at%, which is lower than what can be accurately resolved by regular EDX measurements<sup>77</sup>. In addition, an EDX measurement in this system typically takes a few minutes<sup>77</sup>. Although there are methods which could potentially reduce the acquisition time significantly down to tens of seconds<sup>90</sup>, this is still too long for the time-scale of the measured incubation and layer propagation periods. Beyond aspects of the resolution of the data, the simulations do not have the same hard limitations as the microscope. Examples of this is that flows in the simulation are not limited in the low end by mass flow controllers or the ability for the gas handling system to dilute the precursors to desired levels, nor is it limited in the high end by the need to clean the electron gun more and more often with an increasing pressure inside the microscope column. This enables the simulations to cover a wider parameter range than the experimental setup, which was utilized in Paper iv.

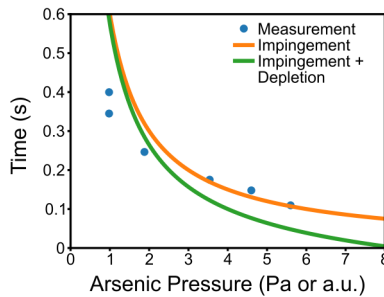


Figure 16: Graph showing layer propagation times from Paper iv, together with a curve representing the propagation being only limited by impingement, as well as a curve which approximates impingement and the initial depletion of the supersaturated droplet.

The benefit of in-situ  $\epsilon$ TEM growth is obvious; it enables the observation of true nanowire growth as it is happening. While the data from the simulations are 100% accurate representations of their simulation framework, the simulation frameworks are not a 100% accurate representation of reality. Thus, the ability to match experimental data and simulated data is immensely beneficial for improving the simulation frameworks, and bringing it closer to reality.

Throughout my time developing the simulations frameworks, it has become clear that many of the trends in the outputs of the simulations are quite robust, meaning that they are not particularly sensitive to the values used for the variables\*. However, this is not the case for the layer propagation times studied in Paper iv. The layer propagation time was highly

\*Although there must be some correlation between some of the variables, e.g. the As flow and the evaporation efficiency.

sensitive to the specific values used, making this data highly useful for improving on the model.

This sensitivity stems from the layer propagation time predominantly being limited by the availability of As, and the concentration of As atoms in the seed particle is typically very low. To a first approximation, the layer propagation can be thought of as limited by the impingement of As. However, as is exemplified in Figure 16, this leaves the layer propagation time to be inversely proportional to the flow of As. This curve is too steep compared to the experimental trend, suggesting that this first approximation does not capture the necessary features.

Instead, the layer propagation time is typically depending on three questions: What is the impingement rate of As on the surface of the particle? How much of this impinged As is evaporated during the layer propagation? How much of the layer is grown in the droplet depletion, meaning how much excess As was available in the seed particle when nucleation occurs? Depending on the answers to these questions, the trends become very different, and these answers are closely tied to the actual values chosen for the parameters in the simulation. The impingement rate is chosen in the simulations through the input of the vapor pressure of the growth species. However, as was discussed in Sections 1 and 5, this does not take e.g. the decomposition of the precursor molecules into the pure growth species into consideration. Thus, while it is reasonable to assume that the scaling of the  $\text{AsH}_3$  pressure in the experimental setup is in line with the scaling of the impingement rate of As, the impingement rate in the model has to be treated as a fitting parameter. As another example, if the effective surface energy of the nucleus is too high then a high supersaturation is required to get nucleation. A higher supersaturation can be found if the molar fraction of As in the seed particle is increased, which can be achieved by lowering the evaporation rate. If this is not balanced, and there are too many As atoms in the seed particle after nucleation, this can lead to the excess As being more than sufficient for completing the entire layer in the depletion step, making the layer propagation effectively instant. In the opposite case, when the surface energy is too low, the excess As atoms are very few and the depletion does not contribute to the layer propagation time.

## Varying As Flows

Before going into how the system responds when changing the flows, an important point to remind oneself of is that during stable growth, the averaged effective V/III ratio must be 1. In other words, if there is no change in the material flows to the particle, there should not be any change in the composition of the particle, averaged over several growth cycles. This is shown in Figure 17. This must hold, regardless if the experimental V/III ratio (meaning the  $\text{AsH}_3$ /TMG ratio) is 1 or 1000, as otherwise at least one of the growth species

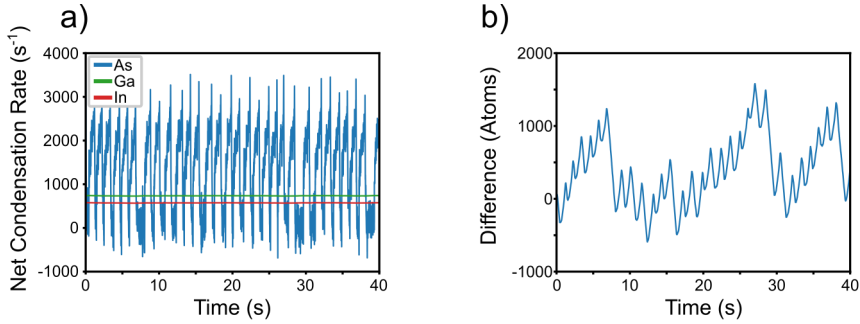


Figure 17: Graph of the net condensation rates for As, Ga and In during a typical ternary simulation (a) and the difference between the group V and group III species of the integrated rates (b). A positive difference represents a relative As accumulation, while a negative difference represents a relative group III accumulation. The integrated rate is approximated by the cumulative sum of the product between each datapoint in (a) and the corresponding time-step for each datapoint:  $\sum_{k=0} J_i[k](t[k+1] - t[k])$ .

will continuously accumulate\* in the seed particle. Throughout my simulations, I have worked in a regime where the V/III ratio was above 1, where all of the arriving Ga atoms are incorporated into the nanowire but a large fraction of the impinged As evaporates away. Though it is reasonable to assume that it exists, I have not worked in a regime where the reverse is true. This means that the influx of Ga would be larger than that of As, and the Ga fraction in the seed particle is kept stable through out-diffusion of Ga. This would require the chemical potential of Ga in the liquid to be on the same levels as the Ga atoms in the adatom phase. Working in this alternative regime could have large effects on the dynamics of the growth, as Ga is much more abundant in the seed particle than As. It is however reasonable to assume that typical MOVPE growth conditions fall in the 'As evaporation regime' which I have simulated. However, the observed dynamics may be different for other III-V materials combinations.

Simulations show that increasing the As flow causes a transient depletion of Ga. This depletion can progress throughout the growth of several layers, depending on the magnitude of the change. During this transient regime, the nucleation is limited by As even if nucleation during the steady state growth is limited by Ga (referring to both the period prior to changing the As flow, and the period after stabilization). As mentioned in Section 6, this combination of As-limited nucleations and a high momentary growth rate generally led to the promotion of WZ. The opposite case, meaning a reduction in the As flow, instead leads to a transient accumulation of Ga which could last for a surprisingly long period of time before settling (several tens of seconds for the flows used in my simulations). An example of this is shown in Figure 18, wherein the As flow is changed back and forth between a high value (which corresponds to the stable growth of ZB) and a low value (which corresponds to the stable growth of WZ) simulated using the framework of Paper II. This figure

---

\*for self seeded growth, e.g. Ga-seeded GaAs growth, an imbalance could also lead to the droplet being continuously consumed until it is gone, ending VLS growth

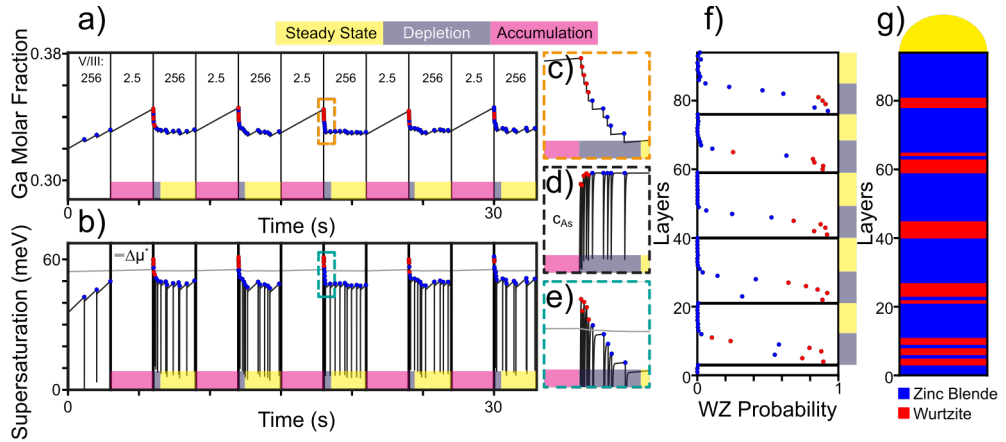


**Figure 18:** Simulation of the growth of a GaAs polytype heterostructure using the model and parameters from Paper II. The As flow alternates between high and low, corresponding to ZB and WZ conditions respectively, in periods of 3 seconds. The Ga concentration is shown in (a), with a zoomed in graph of a transient regime in (c). The V/III ratio of the different regimes are also seen in (a). The As concentration shown in (d) corresponds to the same timeline as (c). The supersaturation is shown in (b) together with the corresponding zoomed in regime in (e). The WZ probability at each nucleation event is shown in (f), and the structure of the final nanowire is shown in (g). Blue (red) dots in panels a-f represent the nucleation of a ZB (WZ) layer. The color bars (steady state/depletion/accumulation) are included as a guide for the eye, to ease the comparison between graphs with different axes.

is intended to highlight not only that the simulation frameworks are perfectly capable of handling transient effects, but also the importance of looking at transient effects in more detail. The As flows chosen for the simulation should, during steady state growth, result in a repeating ZB-WZ superstructure. The output of the simulation does as expected show a repeating ZB-WZ superstructure (with some offset in length between the two structures, matching experimental expectations for crystal structure switching<sup>34</sup>). Thus, it is easy to assume that all growth occurred during steady state. However, the dynamics were very different from the steady state growth as none of the WZ layers were grown during the periods with the WZ conditions. All WZ layers are grown in the transient regime following a switch from the WZ conditions to the ZB conditions. Thus, it is easy to miss some interesting observations just because the results are in line with the expectations.



## 8 Simulating Ternary Nanowire Growth

The addition of one more growth species might seem like a small change at first. However, it does make growth a whole lot more complicated. In addition to wanting the nanowires to grow, in the vertical direction, in the desired crystal structure, while suppressing thin film growth at the substrate and radial growth at the nanowire sidewalls, one also needs to take the composition of the nanowire into consideration. Unfortunately, it is not possible to control these factors individually, since adding a new growth species affects all of these aspects simultaneously. Therefore, the more knowledge we as a community have regarding the growth of ternary nanowires the better. This required a different approach compared to what was used in Papers II- IV, which is the reason for developing the continuous time-line framework used in Paper v. The framework is based on the Au-seeded InGaAs materials system, and this will be the basis of the discussions here.

Many aspects of the growth can be explained through the thermodynamics of the As-Au-Ga-In system. This is clearly exemplified when looking at the simulation of heterostructures, generated using the model of Paper v. Results from simulating a GaAs to InAs heterostructure and a InAs to GaAs heterostructure are shown in Figure 19. These results are in most ways closely related to thermodynamic equilibria between the quaternary As-Au-Ga-In system, the ternary As-Au-(Ga/In) systems and the binary As-Ga or As-In systems. This is perhaps more clearly expressed through the following questions. What is the particle composition during regular Au seeded GaAs growth? What the particle composition during regular Au-seeded InAs growth? At which particle composition is InAs, GaAs and the quaternary particle in equilibrium?

Under typical growth conditions for the binary III-V's from the corresponding ternary seed particle, both Au seeded GaAs and InAs nanowires are grown with the group III component making up around 30 to 50 at% of the liquid seed particle, which can be seen in the first few seconds of Figure 19a and d. For the As-Au-Ga-In system, when using the same parameter space as was used in Paper v, a liquid seed in contact with both GaAs and InAs find equilibrium at around  $X_{In} = 0.3$ ,  $X_{Ga} = 0.03$  and  $X_{As} = 0.003^*$ . This is close to the composition at which the transitions stabilize in the simulations, which is highlighted by the shaded bars in Figure 19a and d.

After the transition has stabilized, the remaining unsupplied group III material (meaning Ga after the GaAs to InAs switch or In after the InAs to GaAs switch) continues to incorporate into the nanowire at low concentrations until the unsupplied group III material has been sufficiently depleted. This occurs quickly for the GaAs to InAs transition, as seen in Figure 19a-c, where Ga is completely removed from the seed particle after around 80 sec-

---

\*while the exact numbers may vary depending on the As concentration (connected to As flow) and temperature, the order of magnitude and general hierarchy of In > Ga > As remains

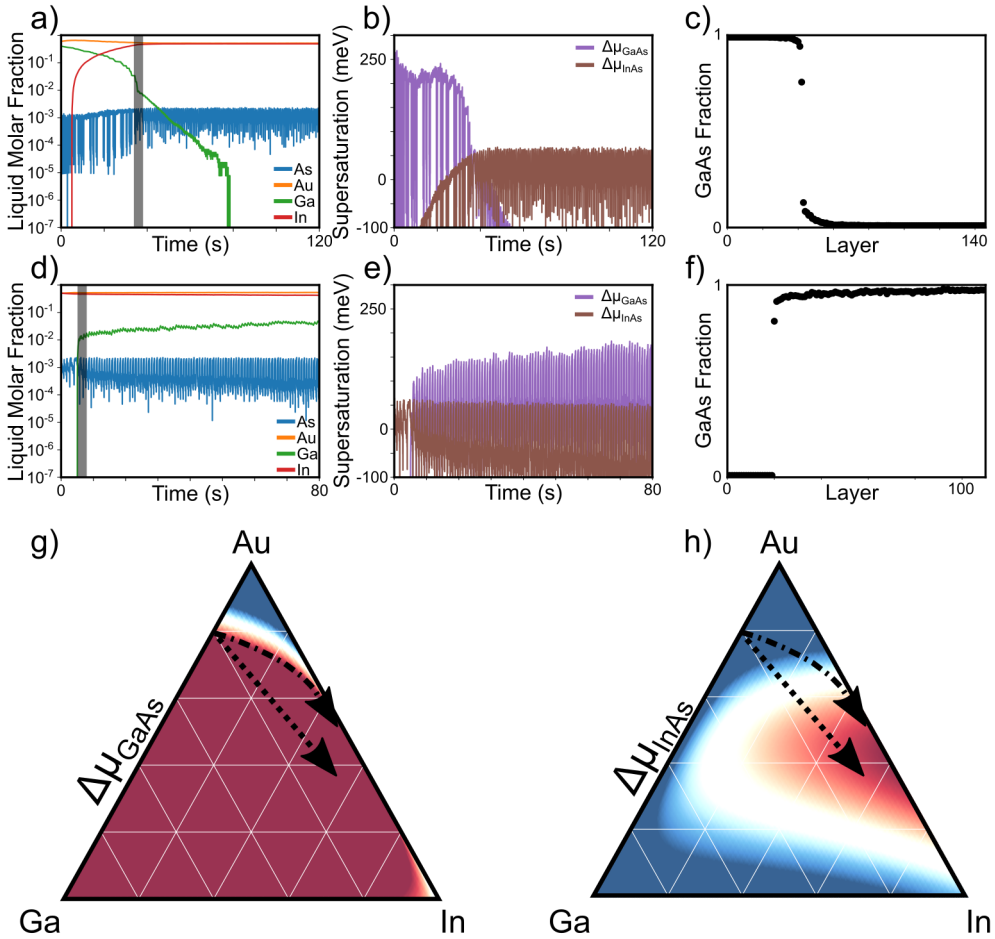


Figure 19: Simulation of a GaAs to InAs heterostructure(a,b,c) and an InAs to GaAs heterostructure (d,e,f). In these simulations, neither strain nor etching rules were used. Pseudo-ternary isothermal diagrams of the supersaturations of GaAs (g) and InAs (h) in a liquid quaternary As-Au-Ga-In system. The molar fraction of As is constant at 0.3 at%, meaning that the corners represents e.g.  $\text{Ga}_{0.997}\text{As}_{0.003}$  and not pure Ga/In/Au. The system is evaluated at  $T=450^\circ\text{C}$ . The color gradient is set to saturate at -100 meV (blue) or +100 meV (red). The dashed line represents the direct compositional change when adding In to a As-Au-Ga seed which is growing GaAs, resulting in supersaturated GaAs. The dot-dashed line represent the path the system will take when following a constant supersaturation of GaAs until a supersaturated InAs is reached.

onds. The depletion happens much more slowly in the reversed direction, see Figure 19d-f, where there is a significant In fraction in the seed and a significant InAs-supersaturation throughout the entire simulation. As a result, In keeps getting incorporated, albeit at a low fraction, into the wire.

The discrepancy between the different equilibria, one where a binary III-V is in equilibrium with the ternary liquid, and one where both the two binary III-V's are in equilibrium with a quaternary liquid, determine much when it comes to the dynamics of the transition.

Going from InAs growth at say  $X_{In} = 0.3$  and  $X_{As} = 0.003$  to GaAs growth at  $X_{In} = 0.3$ ,  $X_{Ga} = 0.03$  and  $X_{As} = 0.003$  only requires a bit of Ga to be incorporated into the seed particle. As the particle does not need to change much, it is reasonable to assume that the particle will remain stable during this transition (stable in the sense that there is no rapid shrinking or swelling of the particle which might unpin it from the top of the nanowire<sup>91</sup>). The downside is that the particle will have a high molar fraction of In in the droplet, which may make it difficult to eliminate In from being incorporated into the nanowire after the transition has been made.

Going from GaAs growth at  $X_{Ga} = 0.3$  and  $X_{As} = 0.003$  to InAs growth at  $X_{In} = 0.3$ ,  $X_{Ga} = 0.03$  and  $X_{As} = 0.003$  is a much larger change where most of the Ga needs to be replaced with In before stabilizing the growth. Interestingly, incorporating In into the Ga-rich seed particle actually increases the supersaturation of GaAs which aids in the depletion of Ga from the droplet. This is shown in Figure 19g and h, which highlights what happens to the supersaturation of both GaAs and InAs when adding In to the As-Au-Ga system. A straight line towards In (dotted in the figures) pushes GaAs deeper into the supersaturated (red) regime. More GaAs will then be grown before InAs becomes supersaturated, leading to the more realistic composition change indicated by the dot-dashed arrows. This transition introduces some different nuances to the growth, which might make it less stable. This is because the nucleation of GaAs essentially becomes In-limited, and the In does not get consumed during this growth. These differences between the two transitions might explain why it seems easier to grow a vertical GaAs on InAs heterostructure than a InAs on GaAs heterostructure without kinking<sup>92,93</sup>.

With this knowledge from the thermodynamics of the quaternary liquid, and how the nanowire growth responds to switches in the material flows, the focus will now be on the steady state growth. In the ternary simulations presented in Paper v, a few results are persistent. A main result is that the nucleation always seemed to progress via pure or close to pure InAs nuclei. This can be seen in the compositional evolution of several individual layers shown in Figure 20. This behavior can easily be motivated by two generally accepted facts; one is that InAs nanowires have a lower sidewall surface energy compared to GaAs, and the other is that for a stable nucleus which is 'sufficiently large', the surface energy becomes insignificant compared to the supersaturation as the nucleus has become more bulk-like. While a nanowire-layer can not really be considered bulk-like, the total surface energy of the nucleus has recently been suggested to actually become lower as the final parts of the layer grows to completion<sup>73</sup>. This suggests that in order to achieve roughly equal attachment rates of GaAs and InAs pairs to a growing layer, the supersaturations of the two must be roughly equal as well. With supersaturations at the same range for GaAs and InAs, and a significantly lower sidewall surface energy of InAs, this leads to nucleation happening via a very InAs-rich critical nucleus. As each binary III-V material comes with its own sidewall surface energy, it is very likely that this behavior should be found in other



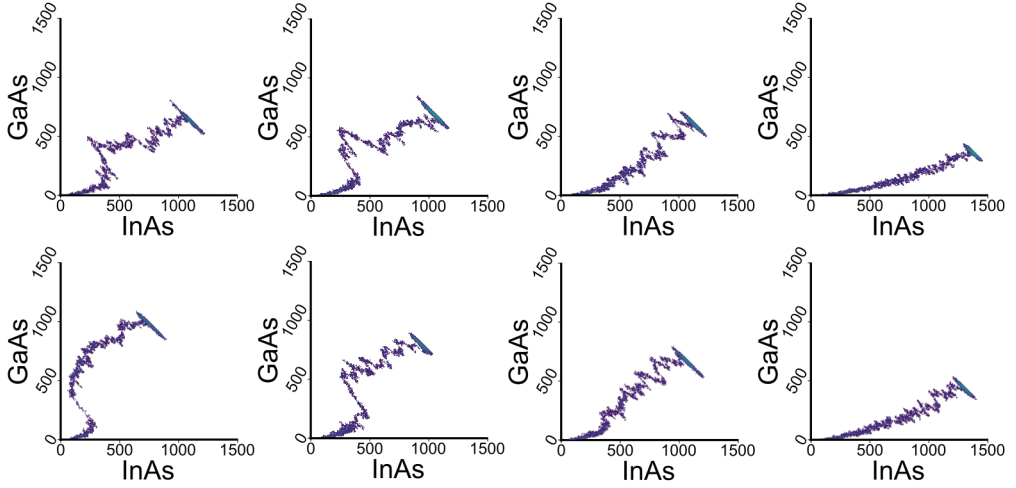


Figure 20: Several heatmaps tracing the compositional path through which the growing nuclei evolved over individual layers during the simulation of InGaAs nanowire growth. Common for all composition-paths is the initial InAs-rich segment.

systems as well.

This behavior leads to an interesting difference between my binary GaAs growth simulations and my ternary InGaAs growth simulations. For binary growth (in the high V/III regime where the simulations have mostly taken place), the composition of the seed is determined solely by the flow of As. As discussed in Sections 6 and 7, in the simulations I find that the As concentration in the seed particle during incubation is determined by impingement and evaporation. The average steady state Ga concentration is then uniquely determined by this As concentration\*. When the As flow is changed, the Ga concentration follows in a predictable manner. For the ternary case, because nucleations occurred via InAs, the As flow did not uniquely determine the seed composition. The flow of As determined  $\mu_{As}$ , which in turn pinned the average  $\mu_{In}$  to maintain a balanced nucleation rate. This means that  $\mu_{Ga}$ , and thus  $X_{Ga}$ , is not pinned in the same way as it was for the binary case. In essence, this means that GaAs growth can to a large extent be controlled via the As flow. InGaAs growth, however, is controlled via the combined As-, In- and Ga flows.

Similarly to what was found in Paper IV for GaAs, the layer propagation is found to be limited by As. However, the composition of the solid layer is found to be most sensitive to variations in the Ga concentration. This is a result of the compositional hierarchy found in the simulations ( $X_{In} > X_{Ga}$ ), and the flow hierarchy used in the simulations ( $J_{Imp,In} \approx J_{Imp,Ga}$ ). Following the same line of thought as in Paper II (but with two components with different fractions instead of two nanowires with different sizes), small variations in

---

\*of course other factors such as temperature and seed material matter, but these remain constant during the simulations

the number of Ga atoms in the seed particle leads to large variations in  $\Delta\mu_{GaAs}$  whereas  $\Delta\mu_{InAs}$  changes very slowly when adding In atoms. From a temporal point of view,  $\Delta\mu_{GaAs}$  increases much more rapidly with time compared to  $\Delta\mu_{InAs}$  during the incubation periods. As a result, it is fair to say that the simulations showed that in the liquid to solid transition, nucleation was In-limited, layer propagation was As-limited, and the Ga-fraction in the solid nanowire was Ga-limited.

While the layer to layer compositions could vary greatly, and vary depending on the settings used in the simulations, the average composition of the nanowire was found to be the same as the ratio of the net impingement rate between Ga and In. Thus, it is important to keep in mind that if one is interested solely in the nanowire composition, then the simulations suggest that focus should be placed on the vapor to liquid transition.

One of the most interesting results to me from the work on InGaAs, was that the inclusion of strain into the simulations induced oscillations whenever the energy of the strain was set to be large. One could imagine such an outcome due to spinodal decomposition, wherein a mixed InGaAs nanowire could lower its energy by separating into In-rich segments and Ga-rich segments. However, these oscillations were found to be a result of the dynamics of the seed particle and not on the thermodynamics of the nanowire. Because nucleations were found to occur via an InAs nucleus, having a large effect of strain meant that any deviations from the average ended up being amplified. A longer than average incubation period led to an above average  $X_{Ga}$ , meaning that the layer should end up being Ga-rich. A Ga-rich layer makes it more difficult to nucleate InAs, leading to an even longer incubation period, and an even more Ga-rich layer. On the other hand, an In-rich layer meant that nucleation required less  $\Delta\mu_{InAs}$ , resulting in a faster than average nucleation and as a result, the layer becomes In-rich. This continues until a tipping point is reached, either because  $X_{In}$  is sufficiently high to nucleate on pure GaAs, or too low to nucleate on pure InAs. These oscillations have to my knowledge, not been reported for experimental growth of InGaAs nanowires, and thus one can assume that it should not occur for the InGaAs system. This might be because the mismatch is not large enough to induce the oscillations, or that there is slightly more GaAs active in the critical nuclei than the simulations suggest, which would alleviate some of the strain. However, as there is a logical and natural explanation for the oscillations, it makes it interesting to consider if it could be induced in other materials systems.

Finally, in regards to the results of Paper v, it is (again) worth highlighting that something which is seemingly insignificant may have large effects on the outcome in a complex and interdependent growth system. As for the Au seeded InGaAs growth, it seems insignificant to say that growth and etching occurs at the growth front. Yet, as was obvious from the results of Paper v, enforcing this had dramatic effects on the growth dynamics, and a significant narrowing in the distribution of the composition of the layers. When parts of a layer grows with a certain composition, and is then subsequently etched back, it is very likely

that the same composition will again be regrown. The effect of this is that the layer cannot freely reform into the composition which has the minimum global energy, if the layer is not homogeneous, as it is trapped in a local minimum. The only way to escape the local minimum is to wait for more As atoms to arrive, and grow the layer until it is complete.

## 9 Concluding Remarks and Outlook

An interesting aspect of working with my research, worth reiterating, is that the results of the simulations are immaculate. What I mean by this is that the results are a perfect representation of the model that generated them, 100% reproducible, all across the world. This is contrasted by experimental growth, wherein it is well known that process parameters are not directly transferable between different machines, or even the same machine at a different point in time, due to e.g. differences in the reactor geometry, the accuracy of a thermocouple, or the history of the machine. This gives a clarity to the results from the simulations which is not found in experimental growth, and which is highly beneficial when it comes to analyzing the results. The models themselves can be significantly improved upon, in order to better represent what is happening in the MOVPE reactor.

One way to improve the models is to expand them to encompass more aspects of the growth. The end goal of developing the model should at some point be to get as close to experimental growth as possible. If the model does successfully match experimental growth, when the experimental input parameters are used as input for the simulations, then the simulations can truly be used in a predictive manner. For instance, the decomposition of the MOVPE precursors can be added as a separate step, wherein the different dependencies of the decomposition discussed in Section 1 can be included. This, together with allowing surface diffusion and impingement of growth species to happen in parallel, could enable more direct comparisons between the pressures in the simulations and the experimental precursor flows. However, I would say that the models are as limited by uncertainty in the material properties as they are by missing modules. Therefore, my assessment is that it is not feasible at this stage to strive towards a model which matches experimental growth. This statement should be revisited if there is less uncertainty regarding the values for materials properties in the future.

Nevertheless, the results from imperfect models can still be beneficial, even if the models are too simple in some regards. There is clarity in simplicity, as it becomes easier to pinpoint exactly what is causing a certain effect, which is perhaps best illustrated in Papers III and V, where multiple cases or settings were used for this purpose. The ability to turn features on and off makes it easier to determine cause and effect. In a more all-encompassing model, it would be more difficult to find the cause for various trends. For my works, the insights which I have conveyed in my papers should be persistent even if the imperfect models were to improve.

Thus, I believe that my models have brought insights to the research community, especially in regards to the dynamics of nanowire growth and interdependence of the system. By interdependence, I mean that changing one aspect of the growth changes much more than that one aspect. This perhaps is the main, unified conclusion of my works: All else is

never equal. Assuming that all else is equal, is likely to lead in the wrong conclusions. Increasing the flow of As in GaAs growth does more than increase the As concentration in the liquid, whilst keeping all else equal. It induces a transient As-limited nucleation regime where Ga depletes, then resulting in an increased  $X_{As}$  and  $X_{Au}$  and a decreased  $X_{Ga}$ . This leads to changes in the surface energy of the liquid and the contact angle, which affects the nucleation barrier and can lead to a change in the crystal structure selection.

In the papers, I used my models to examine very specific aspects of nanowire growth. However, the knowledge is very much transferable to other material combinations or purposes. It does require one to focus more on the holistic picture of the dynamics of the growth which is presented by the simulations, rather than the details of the result. This will likely represent the largest impact left by my research on the community as a whole; either taking guidance from the direct results and trends I have presented, or applying insights on the dynamic response of the system to a different aspect of nanowire growth. This may help in reducing the trial-and-error attempts needed in the development of new experimental growth recipes.

In general, I would consider the research field of III-V nanowires to be associated with significant risks. The biggest of these is that it might not come to fruition in the sense that III-V nanowire devices, such as tandem solar cells, might never become commercially available and thus not have a direct impact on society. This may be due to issues of integrating nanowires with other platforms, or because alternative materials system may end up outperforming III-V nanowires in some significant way. That being said, it is possible that III-V nanowire research may have larger indirect impacts than direct ones, in the sense that III-V nanowires have already been used as a template for fundamental physics studies<sup>94,95</sup>, and have motivated the development of experimental equipment<sup>89</sup>. From the perspective of my work, there is also a potential that my papers inspire other works of kinetic Monte Carlo simulations, either in the field of III-V nanowire growth or in other fields. One should never underestimate the unexpected ripples that scientific advances may have. I myself have based much of my ternary model on studies on the photon absorption for medical detectors, which is described in Section 2, and have used thermodynamic data in Paper 1 which was developed for the purpose of making jewelry. I am certain that the researchers behind those works did not have me as the target audience.

There is another important aspect of my research, connected to how I have carried out my research, which I would like to highlight. There are numerous advantages of computationally based research. Perhaps the biggest, is the disadvantages of experimental research. The simulations I have been running throughout my research were almost all done using a laptop, which was an OK computer when I first got it several years ago. It is, to say the least, less costly than a cleanroom containing a full MOVPE system both in terms of initial investments and continuous expenses. While I had the ability to use a full MOVPE setup during my research, this is not available for everyone to the same extent that a laptop

is. By developing the simulation framework, and showcasing its potential through my research and my publications, I hope that my work can enable more research to be carried out without the need of costly infrastructure, and thus making III-V nanowire research more available to be carried out by more people.



## 10 References

- [1] J. Wallentin, N. Anttu, D. Asoli, M. Huffman, et al. InP Nanowire Array Solar Cells Achieving 13.8% Efficiency by Exceeding the Ray Optics Limit. *Science*, 339(6123):1057, 2013.
- [2] V. Dagtý and N. Anttu. Modal analysis of resonant and non-resonant optical response in semiconductor nanowire arrays. *Nanotechnology*, 30(2):025710, 2019.
- [3] K. Storm, G. Nyland, L. Samuelson, and A. P. Micolich. Realizing Lateral Wrap-Gated Nanowire FETs: Controlling Gate Length with Chemistry Rather than Lithography. *Nano Lett.*, 12(1):1, 2012.
- [4] D. Wagner, D. R. Novog, and R. R. Lapierre. Simulation and optimization of current generation in gallium phosphide nanowire betavoltaic devices. *J. Appl. Phys.*, 125(16), 2019.
- [5] D. Cherns, S. J. Henley, and F. A. Ponce. Edge and screw dislocations as nonradiative centers in InGaN/GaN quantum well luminescence. *Appl. Phys. Lett.*, 78(18):2691, 2001.
- [6] F. Glas. Critical dimensions for the plastic relaxation of strained axial heterostructures in free-standing nanowires. *Phys. Rev. B - Condens. Matter Mater. Phys.*, 74(12):2, 2006.
- [7] M. Yamaguchi, T. Takamoto, K. Araki, and N. Ekins-Daukes. Multi-junction III-V solar cells: current status and future potential. *Sol. Energy*, 79(1):78, 2005.
- [8] B. M. Borg, M. E. Messing, P. Caroff, K. A. Dick, et al. MOCVD growth and structural characterization of extremely lattice-mismatched InP-InSb nanowire heterostructures. *Conf. Proc. - Int. Conf. Indium Phosphide Relat. Mater.*, 249–252, 2009.
- [9] L. Wen, X. Li, Z. Zhao, S. Bu, et al. Theoretical consideration of III-V nanowire/Si triple-junction solar cells. *Nanotechnology*, 23(50), 2012.
- [10] F. Qian, Y. Li, S. Gradečak, H.-G. Park, et al. Multi-quantum-well nanowire heterostructures for wavelength-controlled lasers. *Nat. Mater.*, 7(9):701, 2008.
- [11] H. J. Joyce, J. Wong-Leung, Q. Gao, H. Hoe Tan, et al. Phase perfection in zinc blende and wurtzite III-V nanowires using basic growth parameters. *Nano Lett.*, 10(3):908, 2010.
- [12] G. Jacopin, L. Rigutti, L. Largeau, F. Fortuna, et al. Optical properties of wurtzite/zinc-blende heterostructures in GaN nanowires. *J. Appl. Phys.*, 110(6), 2011.



- [13] M. Nilsson, L. Namazi, S. Lehmann, M. Leijnse, et al. Single-electron transport in InAs nanowire quantum dots formed by crystal phase engineering. *Phys. Rev. B*, 93(19):1, 2016.
- [14] S. Assali, I. Zardo, S. Plissard, D. Kriegner, et al. Direct band gap wurtzite gallium phosphide nanowires. *Nano Lett.*, 13(4):1559, 2013.
- [15] D. L. Dheeraj, A. M. Munshi, M. Scheffler, A. T. J. van Helvoort, et al. Controlling crystal phases in GaAs nanowires grown by Au-assisted molecular beam epitaxy. *Nanotechnology*, 24(1):015601, 2013.
- [16] T. E. Clark, P. Nimmatouri, K. K. Lew, L. Pan, et al. Diameter dependent growth rate and interfacial abruptness in vapor-liquid-Solid Si/Si<sub>1-x</sub>Ge<sub>x</sub> heterostructure nanowires. *Nano Lett.*, 8(4):1246, 2008.
- [17] K. A. Dick, J. Bolinsson, B. M. Borg, and J. Johansson. Controlling the abruptness of axial heterojunctions in III-V nanowires: Beyond the reservoir effect. *Nano Lett.*, 12(6):3200, 2012.
- [18] J. G. Connell, K. Yoon, D. E. Perea, E. J. Schwalbach, et al. Identification of an intrinsic source of doping inhomogeneity in vapor-liquid-solid-grown nanowires. *Nano Lett.*, 13(1):199, 2013.
- [19] K. a. Dick and P. Caroff. Metal-seeded growth of III-V semiconductor nanowires: towards gold-free synthesis. *Nanoscale*, 6(6):3006, 2014.
- [20] C. Lindberg, A. Whitticar, K. A. Dick, N. Sköld, et al. Silver as Seed-Particle Material for GaAs Nanowires—Dictating Crystal Phase and Growth Direction by Substrate Orientation. *Nano Lett.*, 16(4):2181, 2016.
- [21] J. Wallentin, K. Mergenthaler, M. Ek, L. R. Wallenberg, et al. Probing the wurtzite conduction band structure using state filling in highly doped InP nanowires. *Nano Lett.*, 11(6):2286, 2011.
- [22] J. Wallentin, M. Ek, L. R. Wallenberg, L. Samuelson, et al. Changes in contact angle of seed particle correlated with increased zincblende formation in doped InP nanowires. *Nano Lett.*, 10(12):4807, 2010.
- [23] R. E. Algra, M. A. Verheijen, M. T. Borgström, L.-F. Feiner, et al. Twinning superlattices in indium phosphide nanowires. *Nature*, 456(7220):369, 2008.
- [24] Ö. Danielsson, X. Li, L. Ojamäe, E. Janzén, et al. A model for carbon incorporation from trimethyl gallium in chemical vapor deposition of gallium nitride. *J. Mater. Chem. C*, 4(4):863, 2016.

- [25] C. A. Larsen, N. J. Buchan, S. H. Li, and G. B. Stringfellow. Decomposition Mechanisms of Trimethylgallium. *J. Cryst. Growth*, 102:103, 1990.
- [26] C. A. Larsen, S. H. Li, N. I. Buchan, G. B. Stringfellow, et al. Kinetics of the reaction between trimethylgallium and arsine. *J. Cryst. Growth*, 102(1-2):126, 1990.
- [27] G. B. Stringfellow. *Organometallic Vapor-Phase Epitaxy: Theory and Practice*. Academic Press, 2nd ed., 1999.
- [28] R. S. Wagner and W. C. Ellis. Vapor-Liquid-Solid Mechanism of Single Crystal Growth. *Appl. Phys. Lett.*, 4(5):89, 1964.
- [29] M. E. Messing, K. Hillerich, J. Johansson, K. Deppert, et al. The use of gold for fabrication of nanowire structures. *Gold Bull.*, 42(3):172, 2009.
- [30] D. Allwood, I. Grant, N. Mason, R. Palmer, et al. In situ characterisation of epi-ready III-V substrates for MOVPE. *J. Cryst. Growth*, 221(1-4):160, 2000.
- [31] D. Allwood, S. Cox, N. Mason, R. Palmer, et al. Monitoring epi-ready semiconductor wafers. *Thin Solid Films*, 412(1-2):76, 2002.
- [32] J. Kasahara, M. Arai, and N. Watanabe. Capless anneal of ion-implanted GaAs in controlled arsenic vapor. *J. Appl. Phys.*, 50(1):541, 1979.
- [33] B. Goldstein, D. J. Szostak, and V. S. Ban. Langmuir evaporation from the (100), (111A), and (111B) faces of GaAs. *Surf. Sci.*, 57(2):733, 1976.
- [34] S. Lehmann, D. Jacobsson, and K. A. Dick. Crystal phase control in GaAs nanowires: opposing trends in the Ga- and As-limited growth regimes. *Nanotechnology*, 26(30):301001, 2015.
- [35] M. Tornberg, D. Jacobsson, A. R. Persson, R. Wallenberg, et al. Kinetics of Au-Ga Droplet Mediated Decomposition of GaAs Nanowires. *Nano Lett.*, 19(6):3498, 2019.
- [36] F. Glas, J.-C. Harmand, and G. Patriarche. Why Does Wurtzite Form in Nanowires of III-V Zinc Blende Semiconductors? *Phys. Rev. Lett.*, 99(14):146101, 2007.
- [37] A. I. Persson, M. W. Larsson, S. Stenström, B. J. Ohlsson, et al. Solid-phase diffusion mechanism for GaAs nanowire growth. *Nat. Mater.*, 3(10):677, 2004.
- [38] M. Ljungberg and S.-E. Strand. A Monte Carlo program for the simulation of scintillation camera characteristics. *Comput. Methods Programs Biomed.*, 29(4):257, 1989.
- [39] A. Dinsdale. SGTE data for pure elements. *Calphad*, 15(4):317, 1991.

- [40] J. Y. Shen, C. Chatillon, I. Ansara, A. Watson, et al. Optimisation of the thermodynamic and phase diagram data in the ternary As-Ga-In system. *Calphad*, 19(2):215, 1995.
- [41] F. Bechstedt and A. Belabbes. Structure, energetics, and electronic states of III-V compound polytypes. *J. Phys. Condens. Matter*, 25(27), 2013.
- [42] J. Johansson, Z. Zanolli, and K. A. Dick. Polytype Attainability in III-V Semiconductor Nanowires. *Cryst. Growth Des.*, 16(1):371, 2016.
- [43] V. Pankoke, P. Kratzer, and S. Sakong. Calculation of the diameter-dependent polytypism in GaAs nanowires from an atomic motif expansion of the formation energy. *Phys. Rev. B*, 84(7):075455, 2011.
- [44] N. V. Sibirev, M. A. Timofeeva, A. D. Bol'shakov, M. V. Nazarenko, et al. Surface energy and crystal structure of nanowhiskers of III-V semiconductor compounds. *Phys. Solid State*, 52(7):1531, 2010.
- [45] M. Galicka, M. Buwała, R. Buczko, and P. Kacman. Modelling the structure of GaAs and InAs nanowires. *J. Phys. Condens. Matter*, 20(45), 2008.
- [46] R. Leitsmann and F. Bechstedt. Surface influence on stability and structure of hexagon-shaped III-V semiconductor nanorods. *J. Appl. Phys.*, 102(6):063528, 2007.
- [47] M. Rosini and R. Magri. Surface Effects on the Atomic and Electronic Structure of Unpassivated GaAs Nanowires. *ACS Nano*, 4(10):6021, 2010.
- [48] I. V. Markov. *Crystal Growth for Beginners*. World Scientific, 2003.
- [49] J. Julin, I. Napari, J. Merikanto, and H. Vehkamäki. A thermodynamically consistent determination of surface tension of small Lennard-Jones clusters from simulation and theory. *J. Chem. Phys.*, 133(4):1, 2010.
- [50] J. Johansson, K. A. Dick, P. Caroff, M. E. Messing, et al. Diameter Dependence of the Wurtzite-Zinc Blende Transition in InAs Nanowires. *J. Phys. Chem. C*, 114(9):3837, 2010.
- [51] E. D. Leshchenko, M. Ghasemi, V. G. Dubrovskii, and J. Johansson. Nucleation-limited composition of ternary III-V nanowires forming from quaternary gold based liquid alloys. *CrystEngComm*, 20(12):1649, 2018.
- [52] V. G. Dubrovskii, A. A. Koryakin, and N. V. Sibirev. Understanding the composition of ternary III-V nanowires and axial nanowire heterostructures in nucleation-limited regime. *Mater. Des.*, 132:400, 2017.

- [53] J. Johansson, C. P. T. Svensson, T. Mårtensson, L. Samuelson, et al. Mass Transport Model for Semiconductor Nanowire Growth. *J. Phys. Chem. B*, 109(28):13567, 2005.
- [54] V. G. Dubrovskii. Influence of the group V element on the chemical potential and crystal structure of Au-catalyzed III-V nanowires. *Appl. Phys. Lett.*, 104(5):053110, 2014.
- [55] E. Gil, V. G. Dubrovskii, G. Avit, Y. André, et al. Record Pure Zincblende Phase in GaAs Nanowires down to 5 nm in Radius. *Nano Lett.*, 14(7):3938, 2014.
- [56] V. G. Dubrovskii. Fully Analytical Description for the Composition of Ternary Vapor-Liquid-Solid Nanowires. *Cryst. Growth Des.*, 15(12):5738, 2015.
- [57] V. Dubrovskii, Z. Sokolova, M. Rylkova, and A. Zhiglinsky. Composition and Contact Angle of Au-III-V Droplets on Top of Au-Catalyzed III-V Nanowires. *Mater. Phys. Mech.*, 36:1, 2018.
- [58] F. Glas, J.-C. Harmand, and G. Patriarche. Nucleation Antibunching in Catalyst-Assisted Nanowire Growth. *Phys. Rev. Lett.*, 104(13):135501, 2010.
- [59] C.-Y. Wen, J. Tersoff, K. Hillerich, M. C. Reuter, et al. Periodically Changing Morphology of the Growth Interface in Si, Ge, and GaP Nanowires. *Phys. Rev. Lett.*, 107(2):025503, 2011.
- [60] V. G. Dubrovskii. Refinement of Nucleation Theory for Vapor-Liquid-Solid Nanowires. *Cryst. Growth Des.*, 17(5):2589, 2017.
- [61] M. R. Ramdani, J. C. Harmand, F. Glas, G. Patriarche, et al. Arsenic pathways in self-catalyzed growth of GaAs nanowires. *Cryst. Growth Des.*, 13(1):91, 2013.
- [62] P. Krogstrup, H. I. Jørgensen, E. Johnson, M. H. Madsen, et al. Advances in the theory of III-V nanowire growth dynamics. *J. Phys. D. Appl. Phys.*, 46(31):313001, 2013.
- [63] V. G. Dubrovskii, N. V. Sibirev, J. C. Harmand, and F. Glas. Growth kinetics and crystal structure of semiconductor nanowires. *Phys. Rev. B*, 78(23):235301, 2008.
- [64] U. W. Pohl. *Epitaxy of Semiconductors*. Graduate Texts in Physics. Springer International Publishing, Cham, 2020.
- [65] J. Johansson and M. H. Magnusson. From diffusion limited to incorporation limited growth of nanowires. *J. Cryst. Growth*, 525:125192, 2019.
- [66] F. Glas, M. R. Ramdani, G. Patriarche, and J.-C. Harmand. Predictive modeling of self-catalyzed III-V nanowire growth. *Phys. Rev. B*, 88(19):195304, 2013.

- [67] V. G. Dubrovskii, G. E. Cirlin, I. P. Soshnikov, A. A. Tonkikh, et al. Diffusion-induced growth of GaAs nanowiskers during molecular beam epitaxy: Theory and experiment. *Phys. Rev. B - Condens. Matter Mater. Phys.*, 71(20):5, 2005.
- [68] V. G. Dubrovskii. *Nucleation Theory and Growth of Nanostructures*. NanoScience and Technology. Springer Berlin Heidelberg, Berlin, Heidelberg, 2014.
- [69] V. G. Dubrovskii, J. Barcus, W. Kim, J. Vukajlovic-Plestina, et al. Does desorption affect the length distributions of nanowires? *Nanotechnology*, 30(47), 2019.
- [70] M. B. Borg and L. E. Wernersson. Synthesis and properties of antimonide nanowires. *Nanotechnology*, 24(20), 2013.
- [71] J. Johansson, L. S. Karlsson, C. P. T. Svensson, T. Mårtensson, et al. Structural properties of III-B-oriented III-V nanowires. *Nat. Mater.*, 5(7):574, 2006.
- [72] E. K. Mårtensson, S. Lehmann, K. A. Dick, and J. Johansson. Simulation of GaAs Nanowire Growth and Crystal Structure. *Nano Lett.*, 19(2):1197, 2019.
- [73] J. C. Harmand, G. Patriarche, F. Glas, F. Panciera, et al. Atomic Step Flow on a Nanofacet. *Phys. Rev. Lett.*, 121(16):166101, 2018.
- [74] S. Sakong, Y. a. Du, and P. Kratzer. Atomistic modeling of the Au droplet–GaAs interface for size-selective nanowire growth. *Phys. Rev. B*, 88(15):155309, 2013.
- [75] N. Moll, A. Kley, E. Pehlke, and M. Scheffler. GaAs equilibrium crystal shape from first principles. *Phys. Rev. B*, 54(12):8844, 1996.
- [76] E. Pehlke, N. Moll, A. Kley, and M. Scheffler. Shape and stability of quantum dots. *Appl. Phys. A Mater. Sci. Process.*, 65(6):525, 1997.
- [77] C. B. Maliakkal, D. Jacobsson, M. Tornberg, A. R. Persson, et al. In situ analysis of catalyst composition during gold catalyzed GaAs nanowire growth. *Nat. Commun.*, 10(1):4577, 2019.
- [78] S. Lehmann, J. Wallentin, D. Jacobsson, K. Deppert, et al. A General Approach for Sharp Crystal Phase Switching in InAs, GaAs, InP, and GaP Nanowires Using Only Group V Flow. *Nano Lett.*, 13(9):4099, 2013.
- [79] H. J. Joyce, Q. Gao, H. H. Tan, C. Jagadish, et al. Unexpected Benefits of Rapid Growth Rate for III- V Nanowires. *Nano Lett.*, 9(2):695, 2008.
- [80] G. E. Cirlin, V. G. Dubrovskii, Y. B. Samsonenko, A. D. Bouravleuv, et al. Self-catalyzed, pure zincblende GaAs nanowires grown on Si(111) by molecular beam epitaxy. *Phys. Rev. B*, 82(3):035302, 2010.

- [81] T. Burgess, S. Breuer, P. Caroff, J. Wong-Leung, et al. Twinning superlattice formation in GaAs nanowires. *ACS Nano*, 7(9):8105, 2013.
- [82] R. Sun, D. Jacobsson, I. J. Chen, M. Nilsson, et al. Sn-Seeded GaAs Nanowires as Self-Assembled Radial p-n Junctions. *Nano Lett.*, 15(6):3757, 2015.
- [83] T. Akiyama, K. Sano, K. Nakamura, and T. Ito. An empirical potential approach to wurtzite-zinc-blende polytypism in group III-V semiconductor nanowires. *Japanese J. Appl. Physics, Part 2 Lett.*, 45(8-11), 2006.
- [84] V. G. Dubrovskii and N. V. Sibirev. Growth thermodynamics of nanowires and its application to polytypism of zinc blende III-V nanowires. *Phys. Rev. B*, 77(3):035414, 2008.
- [85] J. Johansson, L. S. Karlsson, K. A. Dick, J. Bolinsson, et al. Effects of Supersaturation on the Crystal Structure of Gold Seeded III-V Nanowires. *Cryst. Growth Des.*, 9(2):766, 2009.
- [86] F. Glas. Chemical potentials for Au-assisted vapor-liquid-solid growth of III-V nanowires. *J. Appl. Phys.*, 108(7):073506, 2010.
- [87] B. Gallois and C. H. Lupis. Surface tensions of liquid Ag-Au-Cu alloys. *Metall. Trans. B*, 12(4):679, 1981.
- [88] J. Johansson, N. C. Overgaard, and M. H. Magnusson. The compositional homogeneity of the metal particle during vapor-liquid-solid growth of nanowires. *Sci. Rep.*, 10(1):1, 2020.
- [89] C. Hetherington, D. Jacobsson, K. A. Dick, and L. R. Wallenberg. In situ metal-organic chemical vapour deposition growth of III-V semiconductor nanowires in the Lund environmental transmission electron microscope. *Semicond. Sci. Technol.*, 35(3), 2020.
- [90] A. R. Persson, M. Tornberg, R. Sjökvist, and D. Jacobsson. Time-resolved compositional mapping during in situ TEM studies. *Ultramicroscopy*, 222:113193, 2021.
- [91] M. Tornberg, K. A. Dick, and S. Lehmann. Thermodynamic Stability of Gold-Assisted InAs Nanowire Growth. *J. Phys. Chem. C*, 121(39):21678, 2017.
- [92] K. a. Dick, S. Kodambaka, M. C. Reuter, K. Deppert, et al. The Morphology of Axial and Branched Nanowire Heterostructures. *Nano Lett.*, 7(6):1817, 2007.
- [93] M. E. Messing, J. Wong-Leung, Z. Zanolli, H. J. Joyce, et al. Growth of straight InAs-on-GaAs nanowire heterostructures. *Nano Lett.*, 11(9):3899, 2011.

- [94] N. Vainorius, D. Jacobsson, S. Lehmann, A. Gustafsson, et al. Observation of type-II recombination in single wurtzite/zinc-blende GaAs heterojunction nanowires. *Phys. Rev. B*, 89(16):165423, 2014.
- [95] M. Nilsson, L. Namazi, S. Lehmann, M. Leijnse, et al. Electron-hole interactions in coupled InAs-GaSb quantum dots based on nanowire crystal phase templates. *Phys. Rev. B*, 94(11):1, 2016.

# Scientific publications

## Author contributions

### **Paper I: Understanding GaAs Nanowire Growth in the Ag-Au Seed Materials System**

I designed and performed the experimental MOVPE growth together with co-authors, using samples prepared by my co-authors. I performed the Scanning Electron Microscopy imaging of the samples and extracted and analyzed the data from these images. I constructed the thermodynamic database with input from co-authors and I performed the thermodynamic analysis. I took lead in writing the paper with input from all co-authors.

### **Paper II: Simulation of GaAs Nanowire Growth and Crystal Structure**

I initiated the project and created the model with input from all co-authors. I performed the simulations and analyzed the data. I wrote the paper with input from all co-authors.

### **Paper III: Effect of Radius on Crystal Structure Selection in III–V Nanowire Growth**

I initiated the project and adapted the model with input from all co-authors. I performed the simulations and analyzed the data. I wrote the paper with input from all co-authors.

### **Paper IV: Independent Control of Nucleation and Layer Growth in Nanowires**

I designed the model used for the simulations, with input from my co-authors. I performed the simulations. I analyzed the results of the simulations and discussed it together with the co-authors in connection with the experimental results that my co-authors had obtained. I



wrote the sections in the paper connected to the simulations and gave input to the writing of the rest of the paper.

### **Paper v: Simulating Vapor-Liquid-Solid growth of Au-seeded InGaAs Nanowires**

I initiated the project and created the model with input from all co-authors. I performed the simulations and wrote the paper with input from all co-authors.